JOURNAL OF GEOPHYSICAL RESEARCH, VOL. 99, NO. B5, PAGES 9117-9135, MAY 10, 1994

The continent-ocean crustal transition across the southwest Greenland margin

Deping Chian and Keith E. Louden
Department of Oceanography, Dalhousie University, Halifax, Nova Scotia

Abstract. This paper examines the complete crustal transition across the nonvolcanic, southwest Greenland continental margin of the Labrador Sea using wide-angle and coincident vertical-incidence seismic profiles. Six ocean bottom seismometers and a sonobuoy record *P* and *S* wave first and multiple arrivals from the crust and upper mantle, which are analyzed by two-dimensional dynamic ray tracing and one-dimensional reflectivity modeling. The resulting seismic velocity model requires that the preexisting 30-km thick continental crust is thinned abruptly to ~3 km across the continental slope, primarily by removal of the lower crust. Farther seaward, the crust thickens to ~6 km primarily through the addition of a high-velocity (7.0-7.6 km/s) layer in the lower crust. This lower crustal layer is 4-5 km thick, extends for a horizontal distance of ~80 km, and is interpreted as partially serpentinized upper mantle. It is overlain by a low-velocity (4.0-5.0 km/s), upper layer which is interpreted as highly fractured upper continental crust. Our model suggests that seafloor spreading did not start until chrons 27-28, 13 Ma younger than previously suggested. This interpretation is supported by two-dimensional modeling of gravity and magnetic data along the refraction line. Our results are consistent with a simple shear mechanism for the initial rifting, with the SW Greenland margin as the upper plate. However, a full characterization of the rifting mechanism must await comparison with a seismic model for the conjugate margin, east of Labrador.

Introduction

A major goal of studying the structure of Atlantic-type, passive continental margins has been to discriminate between different rifting models, especially between pure [*McKenzie*, 1978] and simple [*Wernicke*, 1985; *Lister et al.* 1986] shear mechanisms. A simple shear model invokes a low-angle detachment fault that cuts through the continental crust and separates the resulting margins into asymmetric, upper and lower plate conjugates. The upper plate margin records more thinning in the lower crust and less syn-rift subsidence than does its conjugate, lower plate margin. This model has been supported by the existence of an S-reflector, interpreted as the detachment fault, and a smaller amount of upper crustal stretching as compared to total crustal thinning in the Bay of Biscay [*Le Pichon and Barbier*, 1987] and Galicia Bank [*Boillot et al.*, 1989b, 1992]. On the other hand, the observed overall symmetry of crustal thinning across the restored rift zone for the conjugate margins of Flemish Cap [*Keen and de Voogd*, 1988] and Goban Spur [*Peddy et al.*, 1989] suggests a pure shear, symmetric extension with final breakup closer to one side of the rift zone [*Keen et al.*, 1989]. Finally, it is possible to interpret the rifting of some margins using a mixture of pure shear for the lower crust and lithosphere and simple shear for the upper crust (e.g., Galicia Bank; *Sibuet* [1992]).

Seismic refraction methods have been used in defining crustal affinities on rifted continental margins but mainly for volcanic passive margins where the existence of a high-velocity (7.2-7.5 km/s), lower crust likely represents magmatic underplating formed during the initial rifting [e.g., *Mutter et al.*, 1984; *Holbrook et al.*, 1994]. The initial rifting mechanism, however, is probably best preserved on nonvolcanic margins, where the preexisting velocity signature of the continental crust has not been altered by subsequent volcanic activity. For investigating the nature of rifting mechanisms, refraction methods must delineate the detailed velocity structure from unstretched continent to normal oceanic crust. An example is the Goban Spur margin where recent refraction results suggest a uniform, gradual thinning of both the upper and lower crust (i.e., pure shear) across the margin [*Horsefield et al.*, 1994], which is in agreement with reflection data for the conjugate margins [*Keen et al.*, 1989; *Peddy et al.*, 1989]. On the other hand, the wide zone of thin crust off the Iberia margin bears a velocity structure which is different from normal oceanic crust and therefore is assumed to represent thinned continental crust [*Ginzburg et al.*, 1985; *Whitmarsh et al.*, 1986, 1990]. The existence of a thin lower crustal layer bearing a high velocity of 7.2-7.6 km/s in nonvolcanic margins is interpreted to be either underplated melt [*Reid and Keen*, 1990; *Whitmarsh et al.*, 1990] or serpentinized mantle [*Pinheiro et al.*, 1992; *Reid*, 1992].

The conjugate margins of the Labrador Sea are ideal for the investigation of passive margin formation. Reconstructed positions of the margins can be well constrained from the seafloor spreading history of the basin, given its small overall width [*Srivastava*, 1978; *Roest and Srivastava*, 1989]. The margins are nonvolcanic and exhibit an apparent asymmetry in the shelf/slope morphology, sediment thickness [*Balkwill*, 1987; *Rolle*, 1985], and gravity anomalies [*Woodside*, 1989]. In this paper we present detailed seismic velocity variations and their lithologic and tectonic interpretation for the complete transition from continent to

Paper number 93JB03404.
0148-0227/94/93JB-03404$05.00

ocean crust across the SW Greenland margin of the Labrador Sea (Figure 1). *P* and *S* waves from dense airgun shots penetrating crust and upper mantle are observed on ocean bottom seismometers along a 230-km profile. These data are used to construct a two-dimensional (2-D) seismic model. This model contains a 50-80-km wide transitional zone with a low-velocity upper layer interpreted as thinned upper continental crust and a high-velocity lower layer interpreted as serpentinized mantle. Our data suggest that chrons 27-28 mark the initiation of seafloor spreading in the Labrador Sea and are compatible with a simple shear mechanism for the initial rifting. More detailed constraints on the rifting mechanism, however, must await a seismic model for the conjugate margin, east of Labrador.

Regional Geology and Tectonics

The Labrador Sea forms a northwestward extension of the North Atlantic Ocean, with the main basin about 900 km wide bounded in the west by Labrador, in the east by SW Greenland, and in the north by Davis Strait (Figure 1). The rift-related extension of the Canada-Greenland continent possibly started at ~160 Ma, as evidenced from the dating of coast parallel dike swarms in SW Greenland [*Watt*, 1969]. Final rifting occurred with minimal volcanic activity, leaving less than 800 m of syn-rift extrusive basalts on the Labrador margin [*Balkwill*, 1987]. Features typical for Atlantic-type passive margins are present, including asymmetric shelf/slope morphology and sediment distribution. Less than 4 km of sediments are deposited near the west Greenland margin while the Labrador margin has accumulated up to 11 km of sediments under the shelf [*Tucholke*, 1988].

The seafloor spreading history of the Labrador Sea is documented by magnetic anomaly lineations, with well-defined anomalies observed between chrons 21 and 27 [*Srivastava*, 1978; *Roest and Srivastava*, 1989]. Anomaly lineations older than chron 24-25 are broken by several fracture zones (Figure 1), which are associated with a NW rotation of the spreading axis at anomaly 24-25 when Eurasia separated from Greenland. The less clearly defined and lower amplitude anomalies in areas older than chron 27 have been interpreted by *Roest and Srivastava* [1989] as chrons 31 and

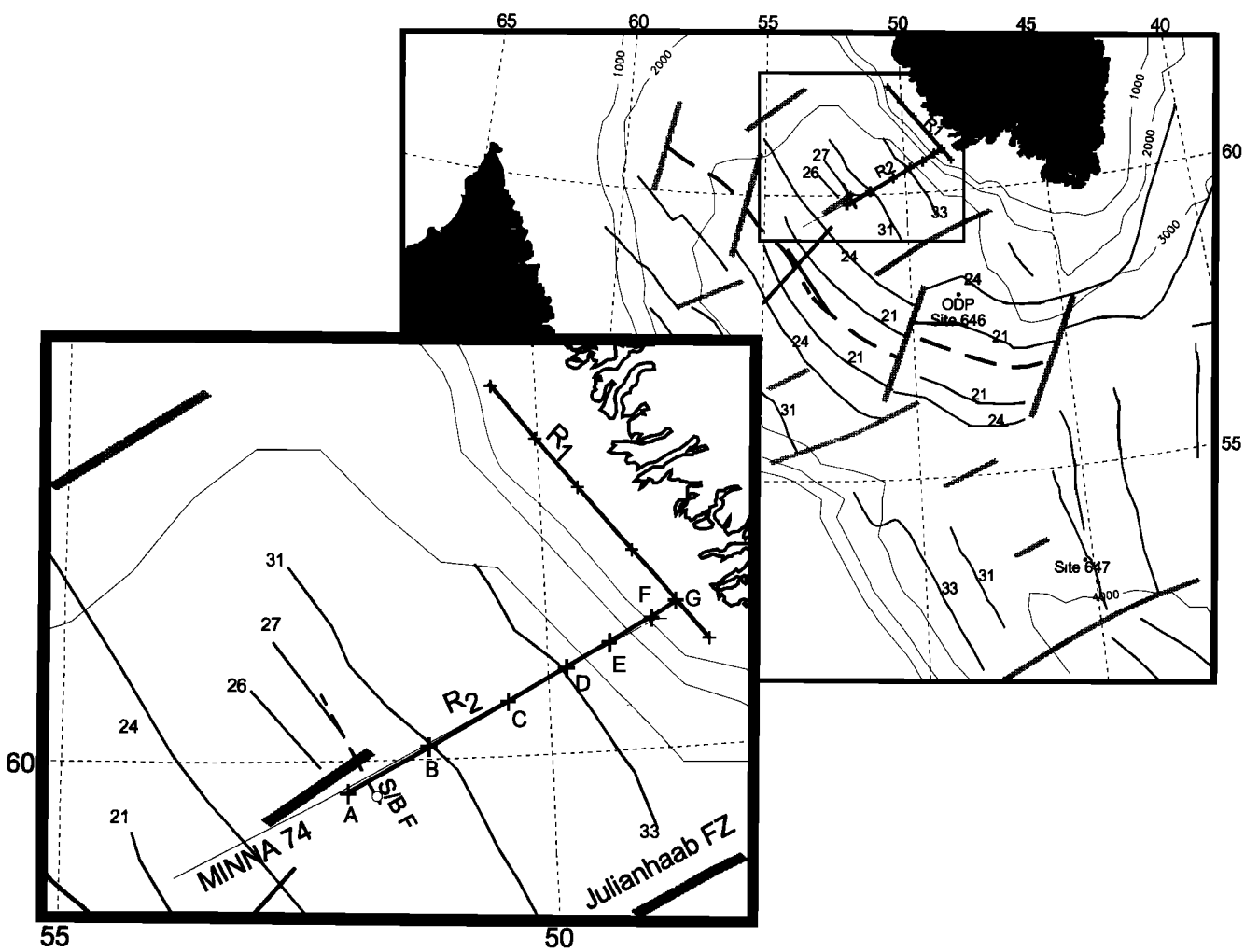

Figure 1. Location map of the Labrador Sea, including bathymetric contours plotted every 1,000 m (dotted lines), numbered magnetic anomalies (thin lines), fracture zones (thick grey lines), and an extinct rift axis (thick broken lines). Refraction lines (thick lines) include R_2 (this paper), R_1 [*Chian and Louden*, 1992], and two lines along and across the extinct ridge axis [*Osler and Louden*, 1992; *Osler*, 1993]. Labeled crosses are OBS instrument locations A-G (Table 1); circle is sonobuoy F [*Stergiopolous*, 1984]. R/V MINNA 74 gravity and magnetic profile is nearly coincident with line R_2.

33. This has been challenged recently by *Chalmers* [1991] who, on the basis of reprocessing of multichannel reflection data BGR-21 (the Federal Institute for Geosciences and Natural Resources), suggested an initiation of seafloor spreading at anomaly 27 (62 Ma). His interpretation places the continent-ocean boundary (COB) ~120 km farther seaward of the previously suggested position.

Recent refraction studies along the shelf of the SW Greenland margin [*Chian and Louden*, 1992] reveal a typical 30-km thick, preexisting continental crust without any magmatic modification. In contrast, 500 km north of this area on the Greenland margin of the northern Labrador Sea, refraction data show the existence of a 5-6-km thick, high-velocity (~7.5 km/s) lower crust, interpreted as magmatic underplating into the lower continental crust during the initial rifting [*Gohl and Smithson*, 1993]. It is likely that this underplating is related to hotspot activity in Davis Strait at chron 25, by which time the central and southern Labrador Sea was already opened. There are scattered, old refraction lines on the northern Labrador margin [*Van der Linden*, 1975] and on the SW Greenland margin [*Stergiopolous*, 1984] to control the deep crustal structure for the Labrador basin. These data, however, do not yield sufficient resolution, and additional deep seismic data are required to further assess the mechanism for the initial rifting.

Reflection Profile

The seismic data we present include wide-angle refraction and coincident single-channel reflection profiles along a 230-km line (R_2) that covers the complete transition from preexisting continental to oceanic crust across the SW Greenland margin (Figure 1). The seismic source for both data sets is an array of six, 1000 in^3 (16.4 l) air guns firing every 90 s with an approximate spacing of 200 m. The reflection data were recorded primarily for constraining the sediment thickness and basement morphology.

The pattern of reflectivity on the single-channel profile (Figure 2) enables a gross definition of three primary seismic sequences within the sedimentary section. The first and the second layers are characterized by high-amplitude reflectors on top and low-amplitude reflectors below. A group of continuous seismic phases forms the boundary between the second and third (bottom) layers. This boundary can be traced continuously from the margin to the east and may correspond to boundary $R_{3/4}$ at Ocean Drilling Program (ODP) Site 646 [*Srivastava et al.*, 1989]. The layer beneath this boundary contains the syn-rift sediments, which are adjacent to the shelf and characterized as strongly folded and faulted seismic sequences (Figure 2).

The most significant feature of the profile is the topography of the basement. In general, the profile shows three zones of distinct basement topography, separated by two basement highs. From the shelf seaward, zone I with large tilted basement blocks probably represents stretched continental crust. At the seaward end of the line (zone III), where magnetic anomalies 26 and 27 are located, reflection hyperbola from the basement are typical of oceanic crust. Zone II in between is characterized by a number of smaller tilted blocks and is interpreted as transitional crust.

As a first-order approximation, the stretching factor for the upper crust β is calculated based on the geometry of the tilted blocks in zones I and II following the method of *Chenet et al.* [1983] (Figure 2). In order to convert two-way travel times into depth, we measured the *P* wave velocities for each sediment layer from sediment-corrected ocean bottom seismometers (OBS) profiles, with reference to the one-dimensional (1-D) modeling results from the sonobuoy data around ODP Site 646 [*Srivastava et al.*, 1989]. A β value of 2.2-3.0 is obtained in transition zone II which is slightly higher than the β value of 2.0 in zone I. The amount of stretching determined in this manner is typically less than the stretching of the crust as a whole. It is likely to represent only the extension in the most brittle layers of the upper crust [*Le Pichon and Barbier*, 1987]. The remaining extension may be accommodated by creep in the lower crust for depth-dependent pure shear models or low-angle faulting for simple shear models.

Wide-Angle Seismic Data and Modeling

Data

Seven OBS were deployed along line R_2, six of them (OBS B, C, D, F, and G) giving useful information. The OBS used along line R_2 record seismic signals from hydrophone and vertical and horizontal 4.5 Hz geophones on cassette tapes. These analog data were digitized and interpolated to a fixed sampling rate of 80 samples per second. Subsequent processing includes band-pass filtering (4-9 Hz for *P* waves and 2-8 Hz for *S* waves), clipping of high amplitudes, and gain that increases linearly with horizontal distance.

Since different recording channels sometimes respond differently to various seismic phases, we find that a sum of several channels is a useful way to present seismograms that demonstrate all prominent phases with just one figure. Before the summation, however, careful correction for the relative time difference between channels is necessary to maintain or enhance the coherency of major seismic phases. In addition, a coherency filter is applied to some of the profiles. This algorithm [*Chian and Louden*, 1992] is defined as a stack of a number of traces along an optimal phase velocity, which produces the maximum semblance within a moving time window of 0.15 s, followed by weighting with the normalized semblance (0-1). The coherency filtering thus defined can be used to enhance certain phases, particularly *S* waves, which are frequently entangled with *P* wave reverberations and multiples (Figure 3).

Major constraints on the crustal velocity structure come from OBS B, C, and D, which provide the best data quality. The data from OBS E are of poorer quality, possibly due to increased noise from deepwater currents. OBS F and G, situated under shallow water (~200 m; Table 1), also give good seismic signals, but the seismic rays are severely distorted by the sharp shelf break and/or the Moho relief, making it difficult to extract crustal information. Because of the failure of OBS A, we used data from an older sonobuoy profile [*Stergiopolous*, 1984] to help constrain the oceanic crustal structure.

One-Dimensional Reflectivity Modeling of Sonobuoy F

The wide-angle profile from sonobuoy F (Figure 4), shot along strike during Hudson 79-013 (Figure 1), is used to constrain the crustal velocity structure at the western end of line R_2. An additional sonobuoy, but with poorer data quality was also deployed at the opposite end of the same profile.

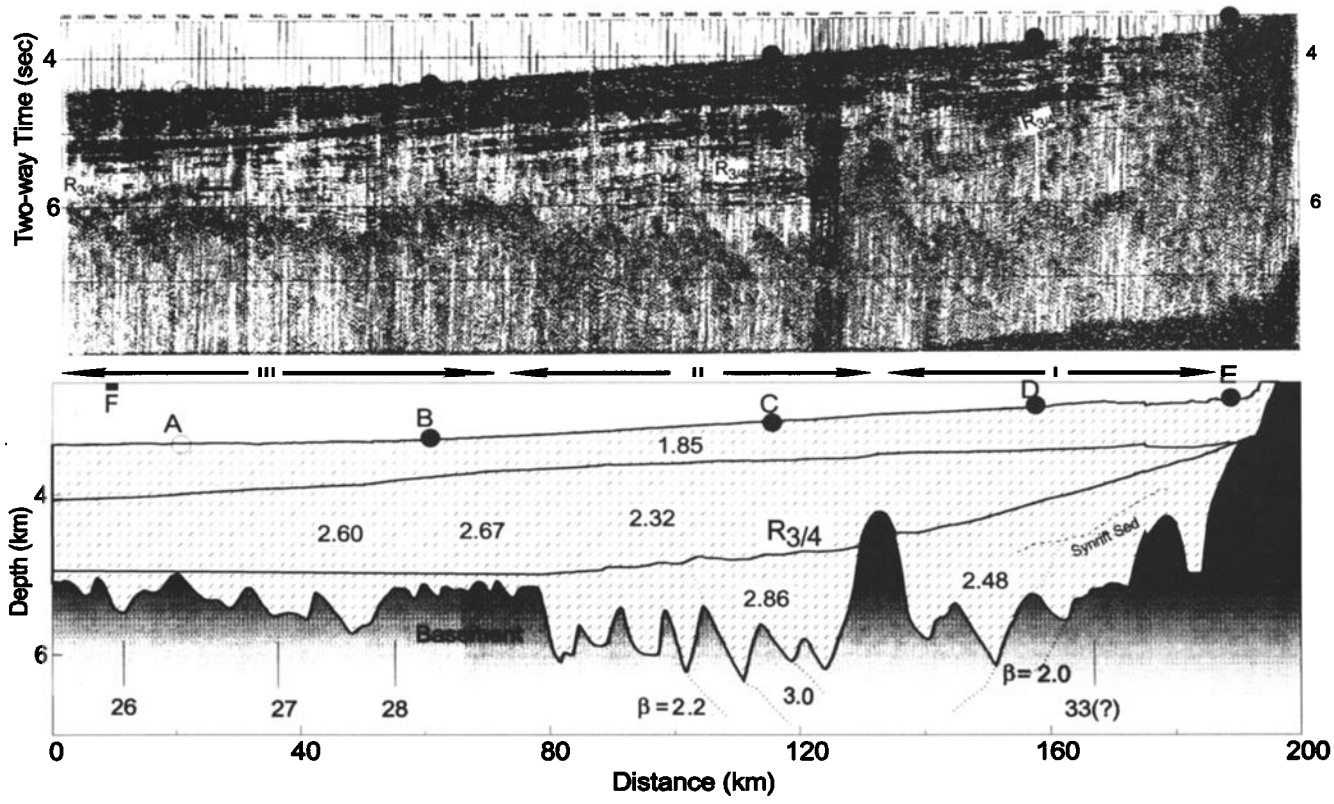

Figure 2. (top) Single-channel reflection data along line R_2 band-pass filtered at 4-40 Hz. $R_{3/4}$ boundary is tentatively interpreted following *Srivastava et al.* [1989]. (bottom) Depth-converted sediment layers and basement topography (see text for details of interpretation). Numbers within sediment layers (hatched pattern) are velocities (in km/s) obtained from OBS profiles along line R_2. Extension factors are calculated from the tilted blocks following *Chenet et al.* [1983]. Magnetic chrons are located and numbered beneath short vertical lines following *Roest and Srivastava* [1989].

Previous slope-intercept analysis of the reversed travel times [*Stergiopolous*, 1984] yielded similar velocity models, indicating a homogeneous structure along the line. In our reanalysis of sonobuoy F, a full waveform record section (Figure 4a) was produced by digitizing the original shipboard FM tape recording. Horizontal ranges were calculated from direct or reflected water waves using an average water velocity of 1.486 km/s. Determination of the P and S wave velocity-depth structure is based on forward modeling of the observed record section using 1-D ray tracing and full reflectivity synthetic seismograms (Figure 4b). Complete velocity-depth values for this model are given in Table 2.

Crustal P phases contain two separate amplitude maxima centered at 13-16 and 17-23 km, with relatively abrupt changes in phase velocity. To fit this pattern requires a blocky structure for the crust, with thicker units of low-velocity gradient at velocities of 5.5, 6.5, and 7.2 km/s, separated by higher gradient zones with variable thicknesses. The initial velocity gradient from 4.8 to 5.5 km/s is not well constrained, apart from the total travel time, on account of the interference of the water reflection with the ground wave. The linear gradient of 1.3 s^{-1} from 5.5 to 6.5 km/s creates the initial amplitude buildup in the refracted wave (P_2), although at ranges slightly less than observed. The sharp discontinuity from 6.5 to 7.2 km/s creates the second-amplitude maximum from the wide-angle reflection (P_3P), although it is not as abrupt or as strong as observed. The depth and velocity transition at the base of the crust is poorly constrained by modeling a third set of phases as P_mP with increasing amplitudes at ranges 27-30 km.

S waves show a similar although less well-developed pattern of amplitudes and phase velocities. The one exception is that the uppermost crustal layer (with V_p=5.5 km/s) must represent a gradient zone (with V_s=3.0 to 3.2 km/s), primarily in order to fit the S wave travel times. The two deeper constant velocity layers are modeled with V_s of 3.6 and 4.1 km/s, giving Poisson's ratios of 0.28 and 0.26 for the mid and lower crust, respectively.

Figure 4b compares velocity models of sonobuoy F with results of 2-D synthetic modeling for a separate profile [*Osler and Louden*, 1992; Osler 1993] which terminates 70 km to the southwest, as located in Figure 1. This comparison indicates that at sonobuoy F: (1) The upper crust is thicker and contains a more complex structure, and (2) The lower crust is of similar thickness but contains a smaller velocity gradient.

Two-Dimensional Modeling of OBS Data

Since significant lateral variations in seismic velocity are expected across the continent-ocean transition, we use 2-D dynamic ray tracing [*Cerveny et al.*, 1977] for modeling the observed OBS data. The sedimentary structure and basement relief used in the modeling are derived from the coincident reflection data (see previous section). We tried two methods for describing the crustal structure. The first one divided the crust into several homogeneous layers using velocities obtained from sediment-corrected sections. The depth of each boundary was varied along the profile to match the observed travel times of crustal and mantle arrivals. This method generated strong wide-angle reflected energy which does not

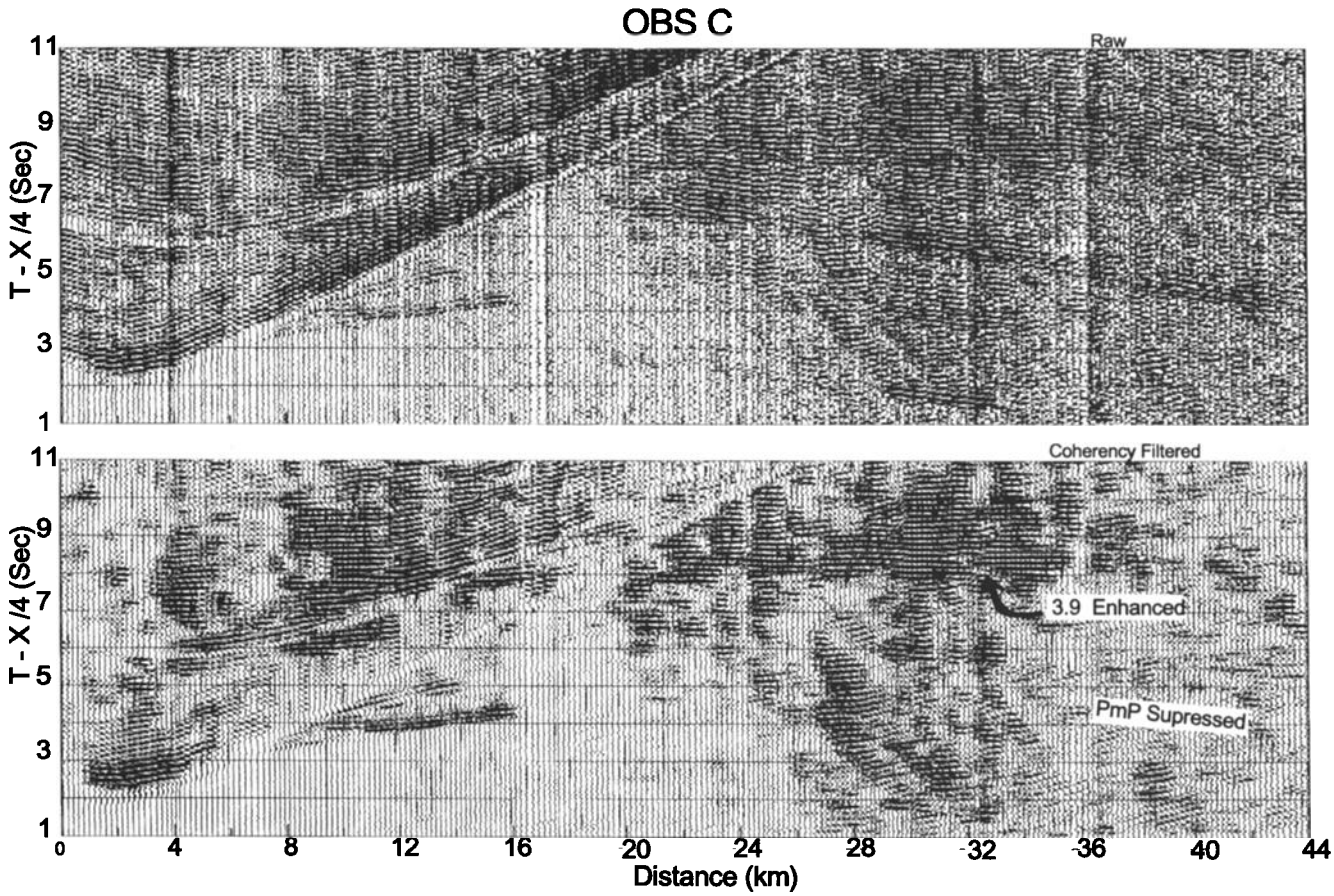

Figure 3. (top) Sediment-corrected vertical geophone channel from OBS C, band-pass filtered (2-8 Hz) with gain increasing linearly with distance. (bottom) Same data with coherency mixing of five adjacent traces. The mixing velocity is scanned between 2.5 and 4.5 km/s at a step of 0.5 km/s.

produce an acceptable fit to the observed amplitudes. Small misfits in travel times also existed. A second approach therefore represented most structural variations by lateral and horizontal velocity gradients. Velocities on a regular grid are obtained by bilinear interpolation of values at arbitrary points.

The seismograms generated from our final, 2-D velocity model with this second method are compared to individual recorded sections for OBS B, C, D, E, and G in Figures 4-8. The strong seismic phases that are crucial in determining the P velocity model include refractions from the sediment layers (P_{sed}), refractions from the upper and the lower crust (P_2, P_3), and reflections and refractions from the upper mantle (P_mP, P_n). In addition, two sets of strong multiples are sometimes useful. The water column multiple (P_mP_2) is frequently strong. Its curvature can constrain the velocity of the lower crust and its travel time the depth of the Moho when the first arrival cannot be recognized (e.g., OBS B; Figure 5). Another prominent multiple (P_mP') is produced between the seafloor and the sediment/basement interface. This multiple is strongest in the hydrophone channel of both OBS B (Figure 5) and OBS C but is minimal, for example, in the horizontal geophone of OBS C (Figure 6).

Table 1. OBS Positions and Water Depths Along Refraction Line R_2

OBS	Latitude, °N	Longitude, °W	Water Depth, m
A	59.8408	52.1033	3368
B	60.0517	51.2900	3303
C	60.2767	50.4233	3076
D	60.4442	49.7767	2916
E	60.5516	49.3514	2823
F	60.6633	48.9100	136
G	60.7400	48.6133	175

OBS B. The velocity-depth structure of crust from the model of sonobuoy F (Figure 4) is used as a control for the western end of the 2-D model. The upper crustal structure is smoothed laterally to provide an overall fit to the western profile of OBS B (Figure 5). The velocity (7.15-7.25 km/s) of the lower crust and the depth (12 km) of the Moho determined from modeling the curvature of P_mP_2 to the west of OBS B are similar to the model of sonobuoy F. The lower crustal velocity east of OBS B is less well constrained because of distortion caused by the sudden basement jump.

OBS C. The seismograms of OBS C (Figure 6) are characterized by significant differences on both sides of the OBS. On the western side, the velocity of the upper crust is about 4.0-5.0 km/s. This low velocity forms a strong velocity contrast with the layers below, producing a distinct reflection phase (P_2P). The lower crust is represented by a clear phase P_3, which is refracted by a gradient layer of high velocity (7.0-7.6 km/s), with the bulk of the lower crust at 7.4-7.6

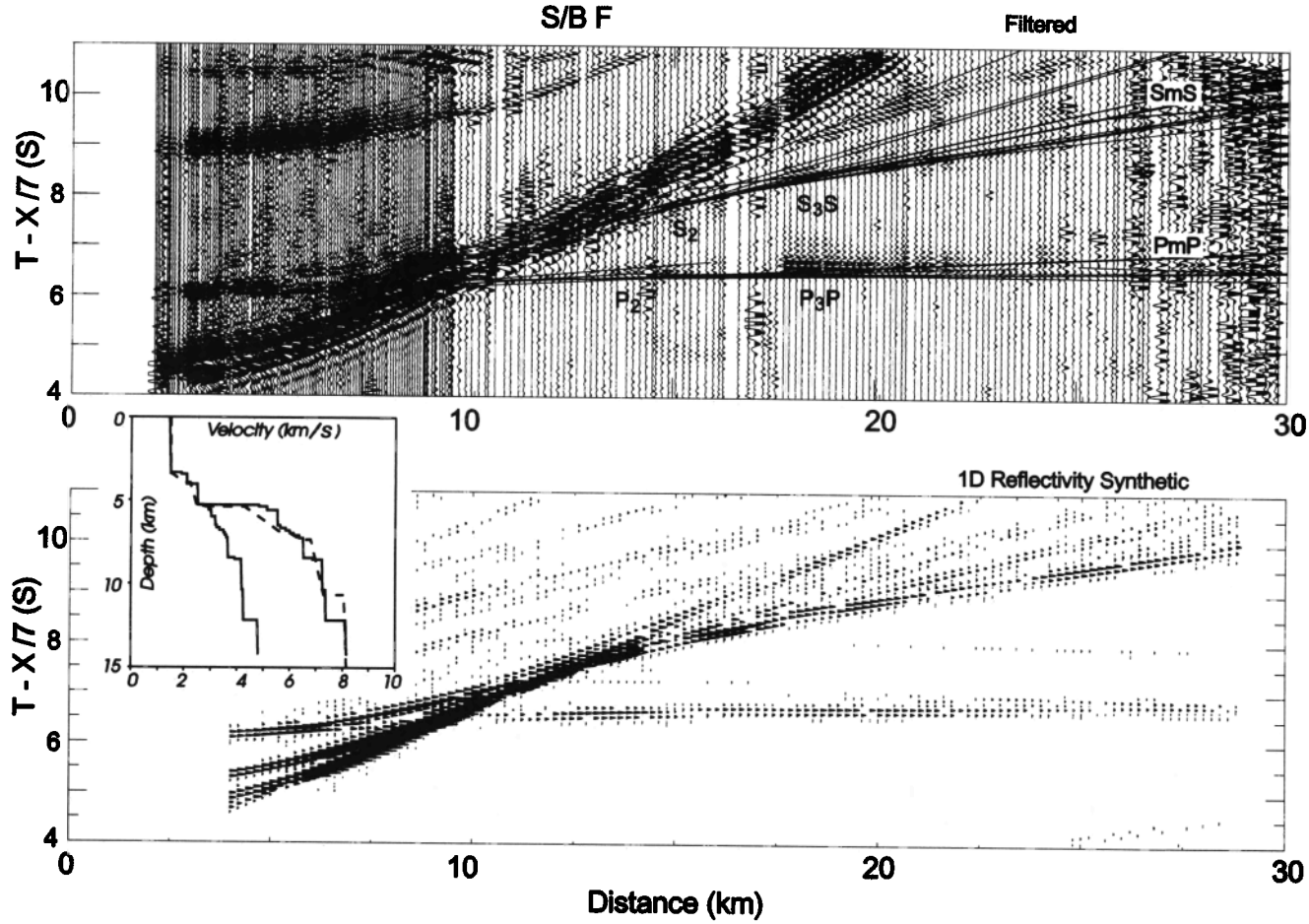

Figure 4. (top) Sonobuoy F hydrophone filtered at 4-10 Hz. Overlain lines are travel time curves computed from one-dimensional reflectivity modeling. Ranges are calculated from direct water wave (not shown) at 0-10 km and from water bottom reflection at 10-30 km, assuming an average water velocity of 1.486 km/s. (bottom) One-dimensional reflectivity synthetic seismograms generated from the *P* and *S* velocity model (solid line) in the upper left corner. Complete velocity-depth values for this model are given in Table 2. Dotted line in the inset shows the *P* velocity structure 70 km southwest of sonobuoy F [*Osler*, 1993]. P_2 and S_2 are refractions from upper crust; P_3P and S_3S are reflections from lower crust; *PmP* and *SmS* are reflections from upper mantle. *S* waves are doubly converted from and to *P* waves at the sediment-basement interface.

km/s. On the eastern side of OBS C, there is a significant travel time pull-down (by 1 s) of upper crustal arrivals between ranges of 12 and 20 km which cannot be fit unless a velocity of ~6.5 km/s is introduced beneath the elevated basement. The high amplitudes of the lower crustal arrival P_3 (at eastern ranges of ~30 km) are produced by the large velocity gradient under this elevated basement. The lower crust under this basement high has a velocity of 6.8-7.4 km/s constrained by P_3 with a phase velocity of ~7.0 km/s. A higher velocity would incorrectly reduce the travel time of P_3. The Moho near the basement high is placed at a depth of 11.8 km which is the same as that westward. This provides a reasonable fit to the travel time of P_mP whose slope is distorted by the faulted basement block east of the basement high. A strong P_mP phase is not observed west of OBS C but is replaced by the clear appearance of P_n which can be traced to a horizontal range of 100 km. The steep tilting of the mantle arrival at a western range of 40 km is caused by the basement jump (>1 km) adjacent to OBS B.

OBS D. The high velocity of the elevated basement is also expressed in the travel time pull-down of lower crustal arrivals of OBS D (Figure 7) at western ranges of 20-28 km. The modeling of P_n for the western ranges of the OBS supports the velocity structures under the basement high as obtained from OBS C. On the eastern side of OBS D, the upper crustal arrival is well modeled and corresponds to an easterly increasing velocity of 5.3-5.6 km/s. First arrivals at ranges >28 km have travel times too early to be produced solely by shallowing the basement toward the continent. A reasonable fit can be produced by setting the Moho at a very shallow depth (~8.2 km) and the mantle underneath with a high velocity gradient (7.7-8.0 km/s). It should be noted that the calculated travel times are slightly earlier than observed. While a smaller velocity of 7.5-8.0 km/s produces a better fit, this would degrade both the calculated travel times for OBS E and the computed gravity anomaly. Therefore complications exist for this part of the seismic model which our data are not sufficient to resolve.

OBS E. Shots to the west of OBS E (Figure 8) give important information on the depth of the Moho. Between ranges of 22-30 km, a strong phase can only be modeled as a refraction from a layer with a velocity of ≥7.7 km/s at 8-9 km

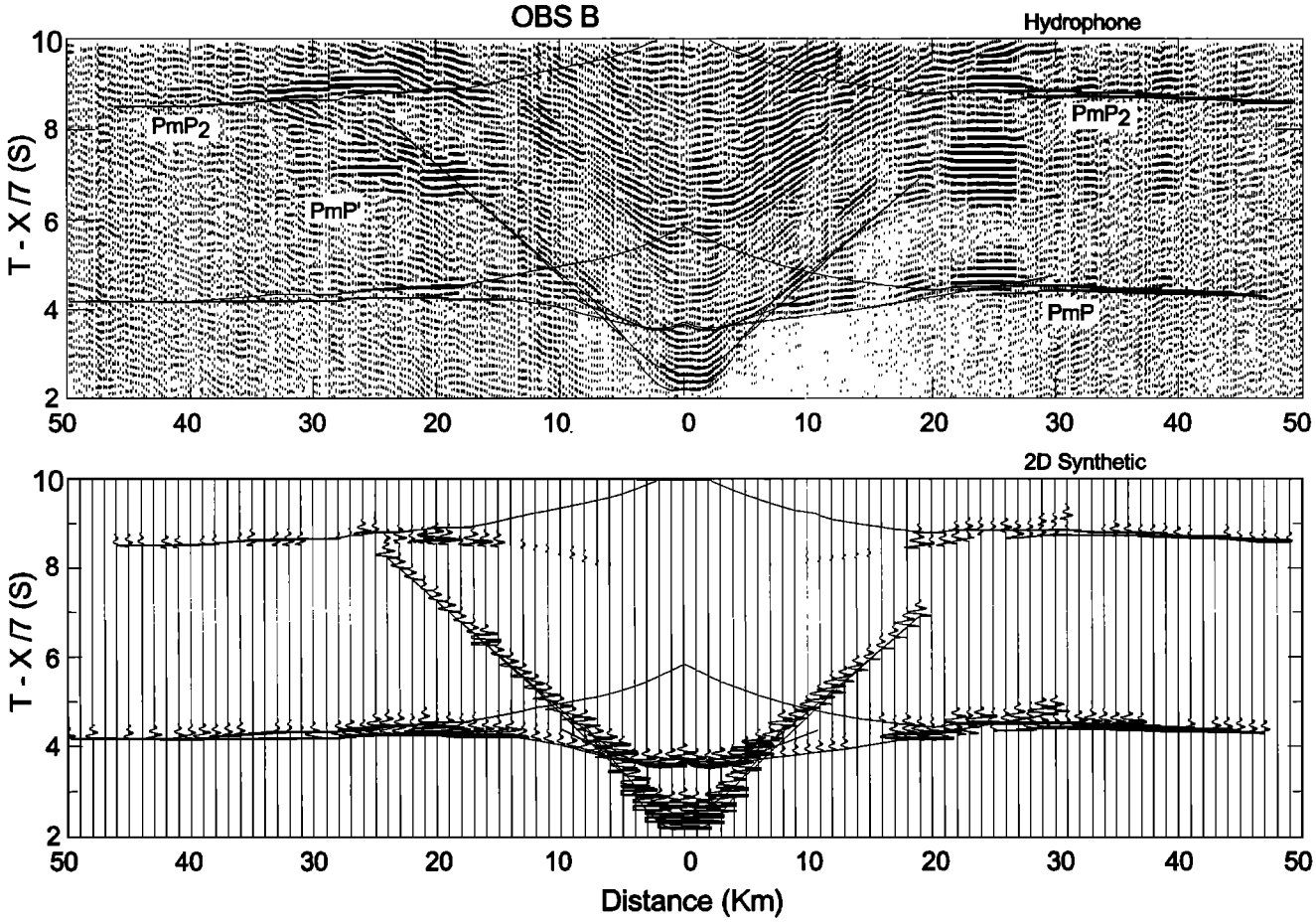

Figure 5. (top) OBS B hydrophone coherency filtered using five traces. Calculated travel time curves from two-dimensional dynamic ray tracing are superimposed. *PmP* is the wide-angle reflection from the Moho. PmP_2 and *PmP'* are water and sediment multiples of *PmP*. (bottom) Synthetic seismograms and travel time curves generated by two-dimensional dynamic ray tracing from the seismic model of Figure 10a.

depth, which is consistent with the modeling of OBS D. A slower velocity will cause an unacceptable travel time delay and will shift the major amplitude westward. To the east, the seismograms are noisy and mostly affected by basement relief across the continental slope.

OBS G. OBS G (Figure 9) is situated at the eastern end of refraction line R_2. *P* and *S* waves from the upper continental crust are observed which give the same velocities as those from another refraction line R_1 along strike [*Chian and Louden*, 1992]. Deeper arrivals are distorted by the sharp shelf break and hence give little information about crustal structure.

The final velocity model that produces all the synthetic seismograms and travel times in Figures 4-9 is shown in Figure 10a. To show the ray coverage for different regions of the model, we plot in Figure 10b the boundaries of the model overlain with ray paths from OBS B, C, D, and E.

Determining *S* Waves

We present the first shear wave data for transitional crust and upper mantle across a nonvolcanic rifted margin. There are primarily two types of crustal *S* waves observed in our OBS data: PSP and PSS (Figure 11). PSP phases are formed by double *P-S* conversion at the sediment/basement boundary.

Table 2. One-Dimensional Velocity Model for Sonobuoy F

Thickness, km	V_p, km/s	V_s, km/s
3.335	1.485	
0.10	1.90	0.58
0.58	2.10	0.64
1.21	2.50	0.85
0.10	4.80	2.70
0.20	5.10	2.90
0.40	5.50	3.00
0.50	5.50	3.15
0.15	5.60	3.20
0.15	5.80	3.30
0.15	5.95	3.45
0.15	6.10	3.50
0.15	6.30	3.55
1.20	6.45	3.60
0.10	6.80	3.85
1.80	7.15	4.10
1.80	7.25	4.15
	8.00	4.70

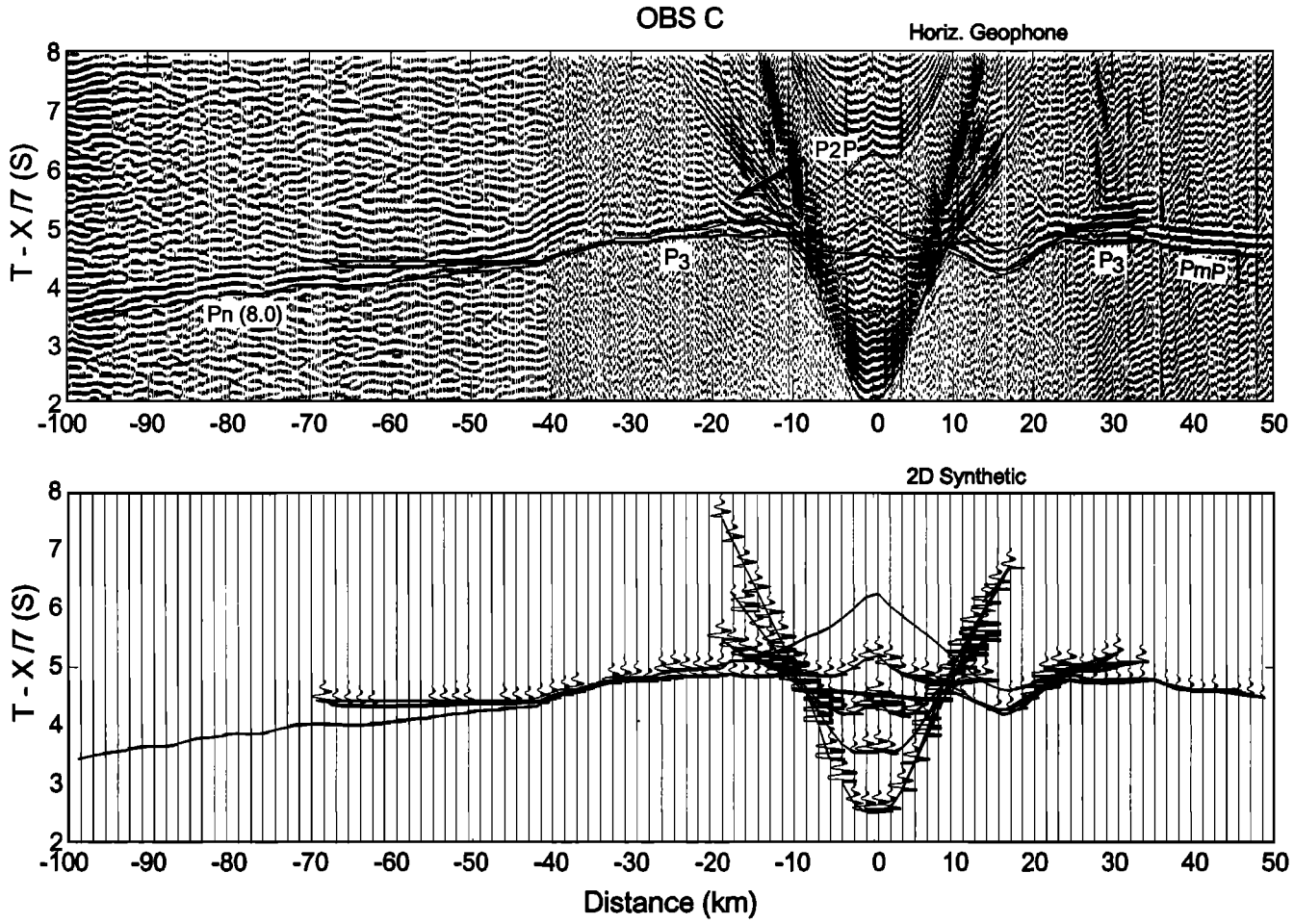

Figure 6. (top) OBS C horizontal geophone with traces between ranges of -100 to -40 km coherency filtered using five traces. Calculated travel time curves from two-dimensional dynamic ray tracing are superimposed. (bottom) Synthetic seismograms and travel time curves generated by two-dimensional dynamic ray tracing from the seismic model of Figure 10a.

The other prominent phase is PSS, which is only converted once. The energy of such converted S waves is especially strong when the P velocity in the bottom of sediments (V_{sed}) is close to the S velocity (V_S) in the crust [*Spudich and Orcutt*, 1980b].

S waves can appear on all component sensors of the OBS. For example, the PSP phase at OBS B only appears on the horizontal geophone (Figure 11a), whereas the PSS phase in OBS C appears on both hydrophone and vertical geophone channels (Figure 11b). Reverberations of P phases frequently interfere with S waves, requiring coherency mixing to suppress phases with higher apparent velocities. In addition, when sediment phases are strong, they interfere with upper crustal S waves because of their similar velocities, making it more difficult to pick the correct S phases.

Once S phases are identified, their travel times are modeled by adjusting the V_P/V_S ratio for all layers of the P velocity model. For OBS B, a V_P/V_S ratio of 1.8 for both the upper and lower crust enables a fit of travel times for PSP and *PSS* (Figure 11a). The modeling of the PSS phase at OBS C requires an additional unknown: the value of V_P/V_S ratio for the top sediment layer. This is determined by maximizing the overall travel time fit. The V_P/V_S ratios for the three sediment layers are 4.5, 2.7 and 1.7. For the high-velocity lower crust and upper mantle, they are 1.83 and 1.90, respectively. This method does not result in a totally satisfactory fit to the data, but it does provide a simple and reasonable estimate of Poisson's ratio for each layer with error estimates (see Appendix). One advantage of this method is that all the structural variations from the better observed P waves are retained for the modeling of S phases, which in general are less complete and definitive.

Error Analysis

Since the final velocity model includes strong lateral and vertical variations with variable seismic ray coverage (Figure 10b), analysis of the resolution of the model can only be investigated for one crustal unit at a time. We perform error analysis for the lower crust but not for the upper crust primarily because the upper crust does not have sufficient ray coverage. Reflections and refractions are treated separately. For a refracted phase, the velocity and top interface depth of a layer are varied to determine their affect on the average travel time misfit. For a wide-angle reflected phase, the velocity gradient and the depth of the bottom interface of the layer are adjusted. When normalized to the misfit endurance (maximum travel time misfit acceptable), these become χ^2 plots where the bounds of acceptable parameters are delimited by the

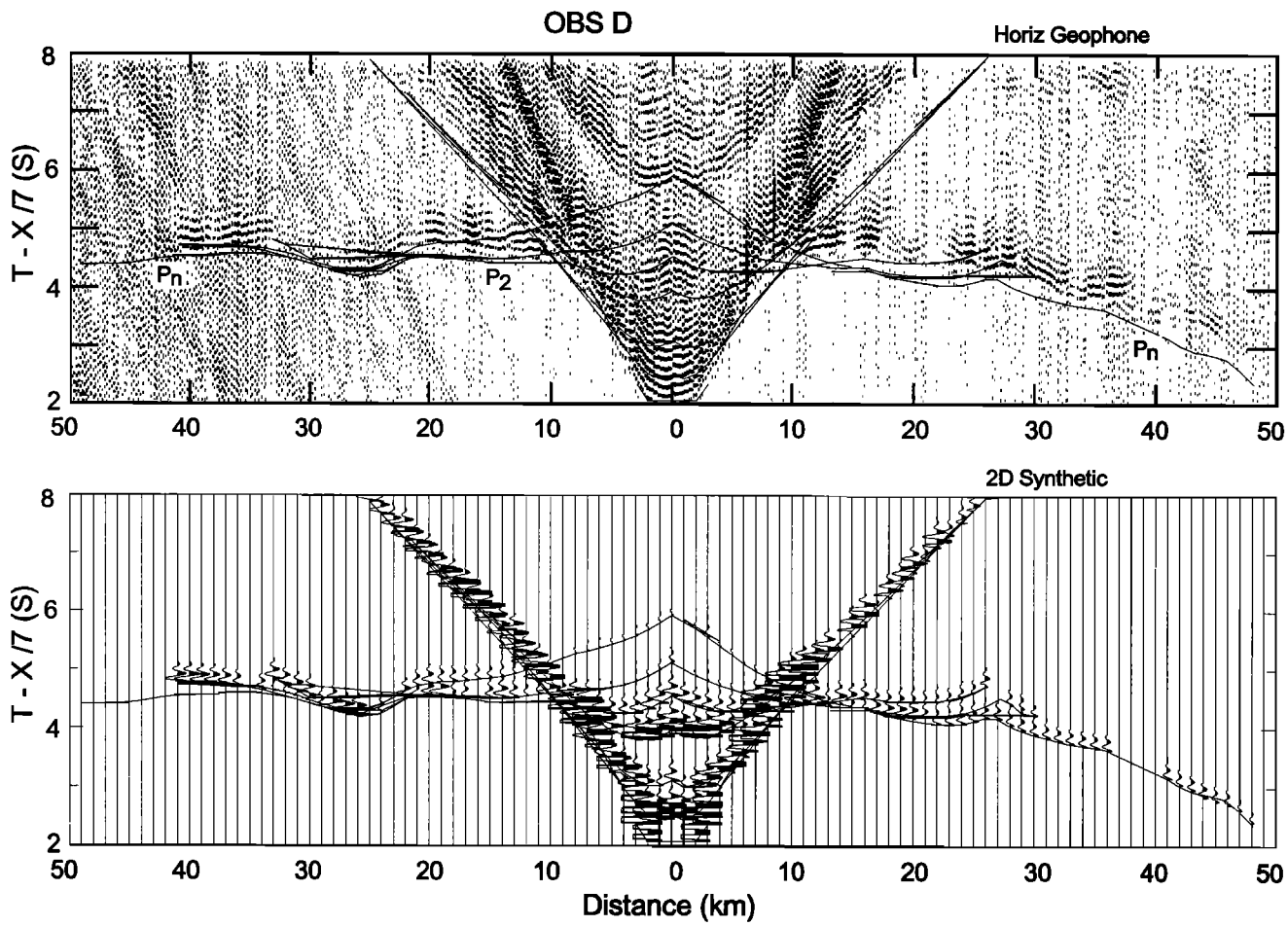

Figure 7. (top) OBS D horizontal geophone. Calculated travel time curves from two-dimensional dynamic ray tracing are superimposed. (bottom) Synthetic seismograms and travel time curves generated by two-dimensional dynamic ray tracing from the seismic model of Figure 10a.

contour of χ^2=1. The details of this method are discussed in the appendix.

Figure A1 gives results of an error analysis for V_p of the lower crust west of OBS C. The contour levels are normalized to 40 ms, which includes the errors in first-arrival travel times. Errors are ±0.10 km/s for V_p and ±0.3 km for the top boundary depth. The same analysis is performed for the P_n phase, which indicates an error of ±0.05 km/s for the upper mantle P velocity and ±1 km for the Moho depth. For a PSS phase at OBS C, error analysis follows a similar approach (see Appendix) which indicates an error of ±0.20 km/s for the lower crustal S velocity (Figure A2).

The errors of P and S velocities for the lower crust west of OBS B are estimated by iterating the 2-D model for OBS B and 1-D reflectivity model for sonobuoy F. By this qualitative approach, we estimate that the errors are approximately ±0.15 km/s for V_p and ±0.20 km/s for V_s. These values are similar to the results of the previous, more quantitative approach.

Gravity and Magnetic Modeling

The gravity and magnetic data used for modeling were extracted from a R/V MINNA 74 profile [*Voppel et al.*, 1988] (S. P. Srivastava, personal communication, 1993), which is almost exactly coincident with our refraction line R_2 (Figure 1). Calculation of synthetic magnetic anomalies are based on the spreading rates of *Roest and Srivastava* [1989] and the time scale of *Kent and Gradstein* [1986]. The observed magnetic data (Figure 12) show a clear change in pattern at anomaly 28. While chrons 25 and 26, and possibly 27 and 28, correlate well with observed anomalies, chrons 31-33 do not. Therefore it is possible that seafloor spreading with the generation of true oceanic crust did not start until chron 28. This is compatible with the interpretation of *Chalmers* [1991].

The gravity map of the Labrador Sea [*Woodside*, 1989] shows small along-strike variations adjacent to line R_2, justifying two-dimensional gravity modeling. The contribution of the sediments is calculated using the drilling results at ODP Site 646 [*Jarrard et al.*, 1989] (see Figure 1 for location) to determine the velocity-density relationship for the top 1 km of sediments. These data are extrapolated downward to cover the entire sediment column. The contribution from the crust is calculated from the velocity grid obtained from the 2-D ray tracing model (Figure 10a), converted into density using the relationship $\rho = -.6997 + 2.2302V_p - .598V_p^2 + .07036V_p^3 - .0028311V_p^4$ [*Ludwig et al.*, 1971]. We set the minimum crustal density as 2.40 g/cm^3 and the maximum as 3.30 g/cm^3. We assume a uniform mantle density (3.30 g/cm^3) and calculate gravity from blocks above 35 km depth.

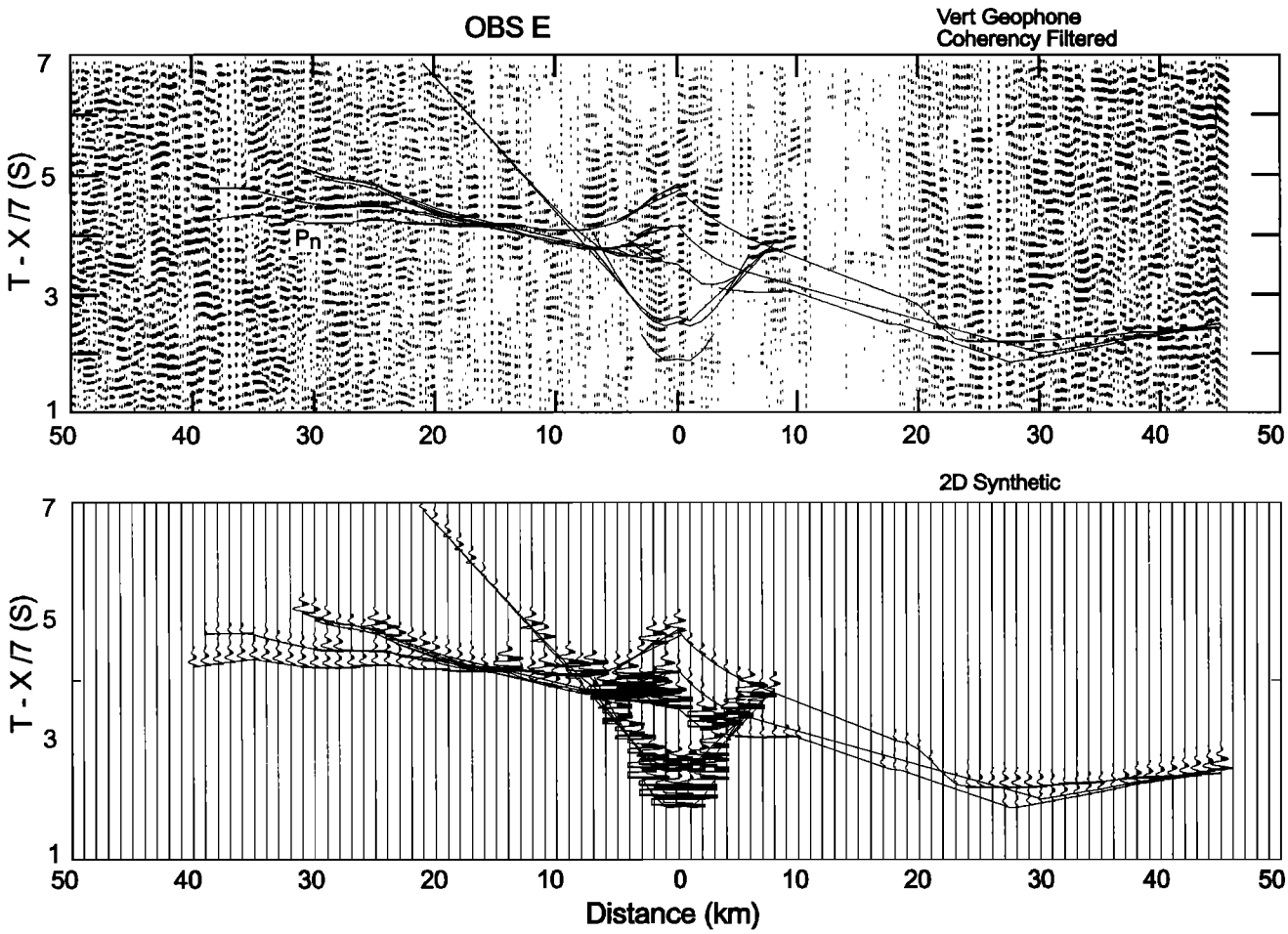

Figure 8. (top) OBS E vertical geophone coherency filtered using five traces. Calculated travel time curves from two-dimensional dynamic ray tracing are superimposed. (bottom) Synthetic seismograms and travel time curves generated by two-dimensional dynamic ray tracing from the seismic model of Figure 10a.

The final computed gravity curve fits the overall patterns of the observed data with a maximum misfit of 5 mGals (Figure 12), which is not significant considering the resolution of the observed gravity profile. Two important controls on the crustal structure result from this model:

1. The observed free air gravity anomaly along line R_2 provides the only control over the shape of the deepening Moho east of OBS E. It is characterized by a positive peak (34 mGals) at the shelf break, followed at 10 km seaward by a large negative anomaly (-63 mGals). This sudden change is primarily due to the edge effect between the abrupt deepening of the basement and the steep slope of the Moho. The calculated gravity low between 180 and 200 km is particularly sensitive to the Moho relief under the continental slope.
2. The model provides important controls over the depth of the Moho at the base of the continental slope. The diagram in the middle of Figure 12 shows two computed gravity curves. The dotted curve results from a Moho which remains flat seaward of the continental slope. A Moho which shallows to 8.2 km at the bottom of the continental slope significantly improves the fit of the gravity (dashed line) and is more consistent with our 2-D seismic modeling, particularly for OBS E (Figure 8).

It can be seen from Figure 12 that the gravity contours follow velocity contours except for the leftmost 50 km of the profile. This exception is introduced because strict adherence to the velocity-density relationship used in the remainder of the model produces a calculated gravity curve for the leftmost 50 km which is ~20 mGal higher than observed. An alternative for avoiding this misfit is to deepen the Moho from 12 to 13 km west of OBS B. While this change of Moho is within the error bounds of our data, it is not supported by any other deep seismic data in the basin.

Discussion

The Seismic Model

The seismic model shown in Figure 10a represents the complete crustal transition across the SW Greenland continental margin. A gross feature of the model is that it can be divided into three distinct zones, similar to those previously identified from basement morphology. In zone I, the 30-km preexisting continental crust is thinned abruptly to a thickness of only ~3 km under OBS E. Further west, this layer terminates at a basement high where it joins zone II, which has a low-velocity upper crust, underlain by an

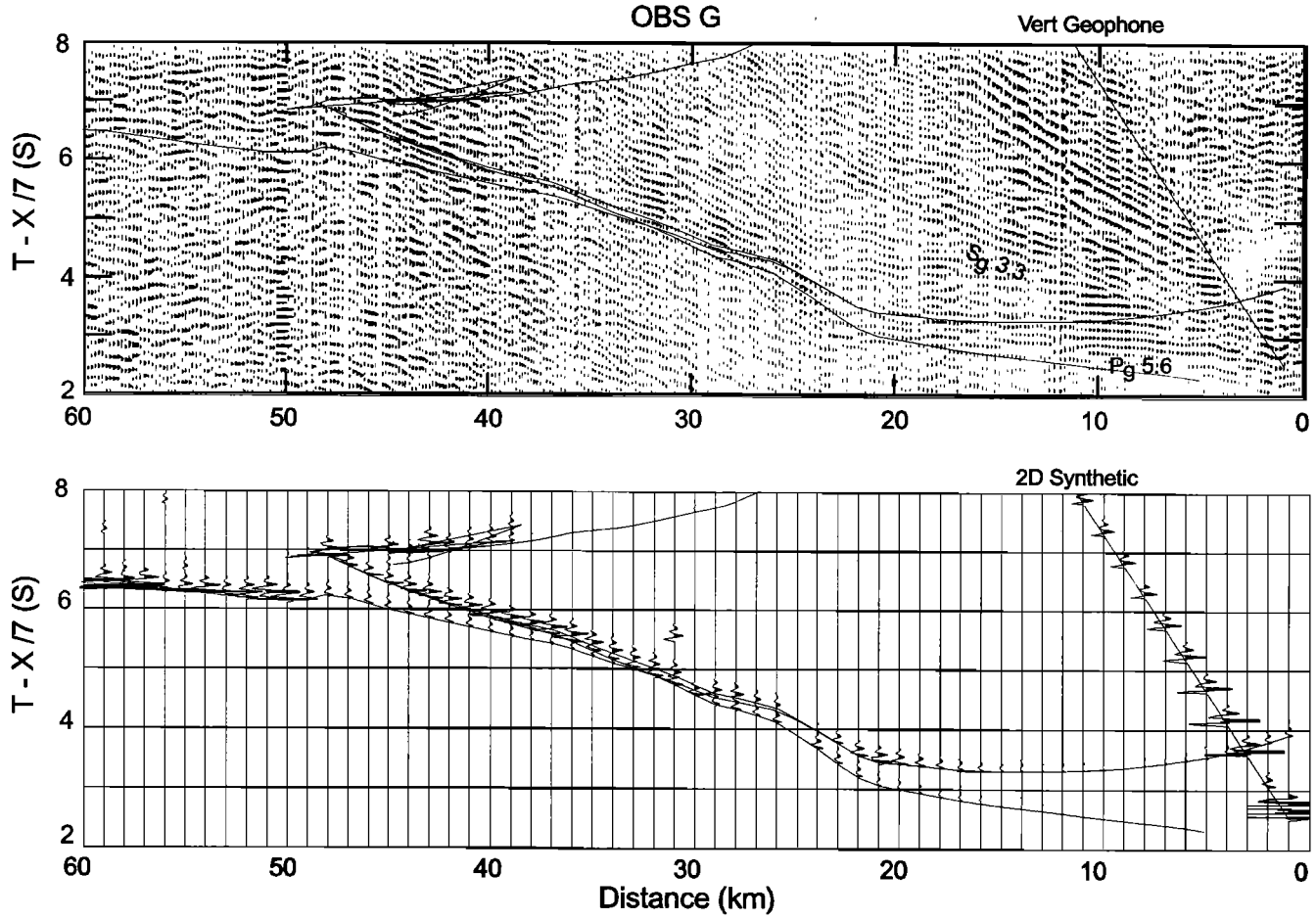

Figure 9. (top) OBS G vertical geophone coherency filtered using five traces. Calculated travel time curves from two-dimensional dynamic ray tracing are superimposed. *Pg* and *Sg* (with associated phase velocities in km/s) are *P* and *S* refractions from upper continental crust. (bottom) Synthetic seismograms and travel time curves generated by two-dimensional dynamic ray tracing from the seismic model of Figure 10a.

unusually high-velocity (~7.5 km/s), 4-5-km thick lower crust. This zone spans a length of ~50 km, terminating in the west at another basement high which separates zone II from a 7-km thick crust bearing oceanic-type velocities (zone III).

Remarkable vertical and lateral variations are observed both in the depths and velocities near the two basement highs that separate the three zones. Among these complexities, the structures around the basement high between zones I and II are the most interesting and important. To the east, the V_p of the upper crust ranges from ~5.5 to ~6.2 km/s. The similarity of this value with that of the adjacent, preexisting, upper and middle continental crust under the shelf [*Chian and Louden*, 1992, Figure 12] suggests that the crust east of OBS D is composed mainly of stretched metamorphosed upper and middle continental crust.

To the west of the basement high, the upper crust in zone II has critical importance in determining the position of the continent-ocean boundary (COB). An evident feature of this upper crust is that the seismic velocity (4.0-5.0 km/s) is unusually low compared to both the continental crust to its east and oceanic crust to its west. Comparison with a recent multichannel reflection profile (*Keen et al.*, 1994), which is adjacent and parallel to our line R_2, indicates that the base of the upper crust in the transition zone is a strong reflective boundary. This reflector is similar to the *S* reflector in the Bay of Biscay [*Le Pichon and Barbier*, 1987], and it can be traced 100 km westward from OBS E . Therefore the upper crust throughout zone II possibly stems from a common origin.

The most surprising result of this work is the existence of a high-velocity (7.2-7.6 km/s), lower crust which is 4-5 km thick within a 50-70 km-wide zone around OBS C. The bulk part of this lower crust has a V_p of 7.4-7.6 km/s with an error bound of ±0.1 km/s (Figure A1). The corresponding V_s is 4.0 ± 0.2 km/s as determined from a PSS phase (Figure 11), which implies a Poison's ratio of 0.30 ± 0.03. This high-velocity layer is restricted in its extent between OBS B and D. Its high velocity (7.4-7.6 km/s) cannot be found either in the continental crust to the east [*Chian and Louden*, 1992] or in the oceanic crust to the west (sonobuoy F, Figure 4; OBS B, Figure 5).

To investigate the origins of the lower crust in zones II and III, a V_p - V_s diagram (Figure 13) is used to compare reported seismic data for the crust and upper mantle [*Christensen*, 1989] with laboratory data for serpentinites and pyroxene/olivine gabbros [*Spudich and Orcutt*, 1980a; *Christensen and Smewing*, 1981]. In addition, we include

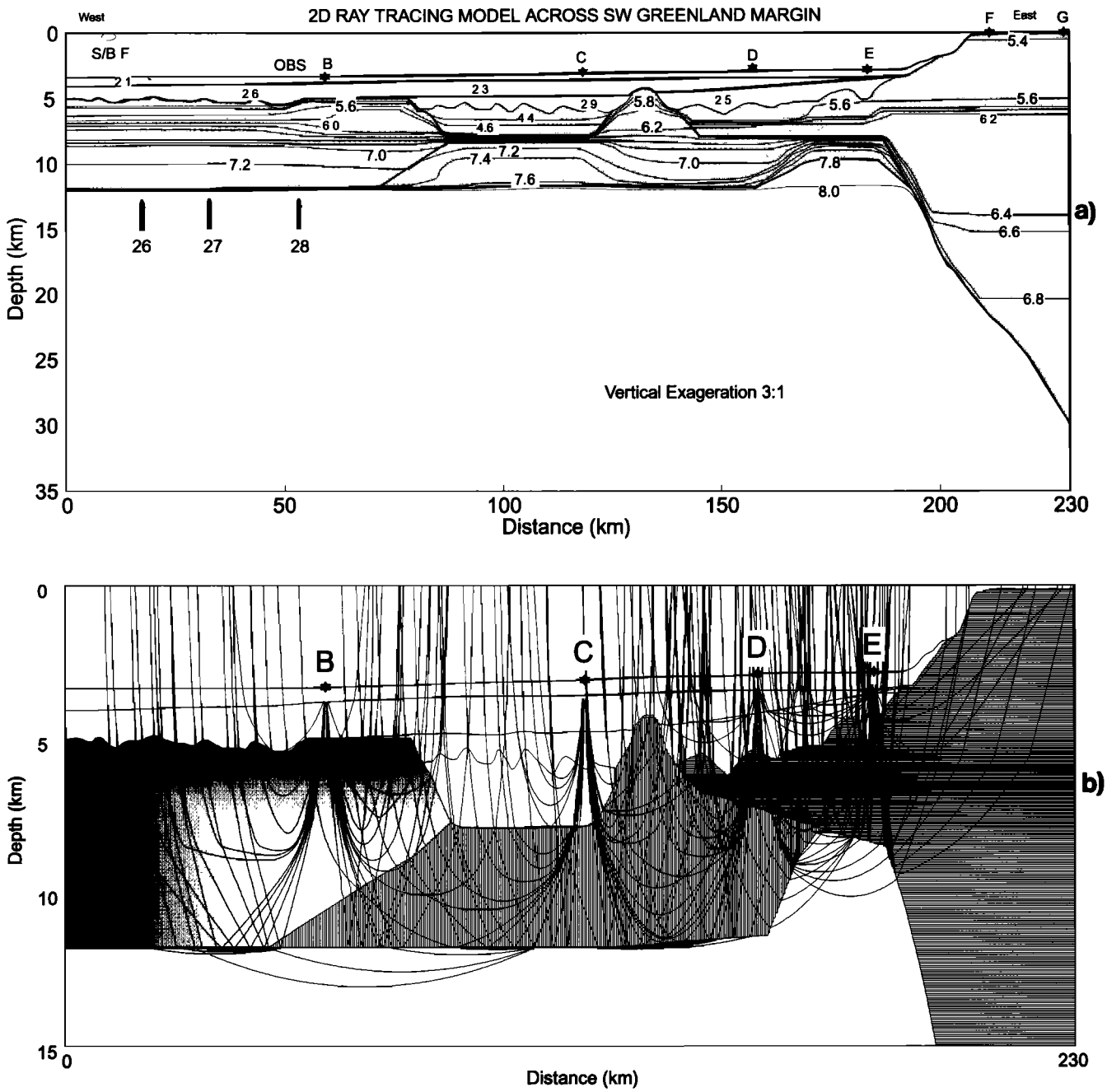

Figure 10. (a) Two-dimensional velocity model showing contours of V_p (in km/s) across the SW Greenland margin. The contour interval is 0.2 km/s. At some significant velocity boundaries (thick lines) contour lines are terminated for clarity. Solid stars indicate positions of OBS; oval delineates the approximate position of sonobuoy F. Vertical exaggeration is 3:1. (b) Selected ray paths for OBS B, C, D, and E overlain by boundaries of the two-dimensional model shown above.

results for the lower continental crust along the SW Greenland shelf determined by *Chian and Louden* [1992]. The observed V_p of the lower crust in zone III is similar to values reported by *Osler* [1993], who shows that rather high velocities (<7.3 km/s) for layer three are typical of the oceanic crustal structure within the Labrador Sea to the east of the extinct rift axis. The even higher V_p for the lower crust of zone II lies outside the region of normal gabbroic crust but is consistent with the V_p observed for the underplated lower crust on volcanic margins. It also intersects the theoretical curve (PSP) for serpentinized mantle [*Christensen*, 1966]. Therefore the velocities alone are not able to definitely distinguish between an underplated melt (i.e., high-Mg mafic gabbro) and serpentinized upper mantle minerologies.

Undercrusted Serpentinite or Magmatic Underplating?

High-velocity lower crust has been found on other nonvolcanic, rifted continental margins, but its lithology and mechanism of formation are similarly not clearly determined.

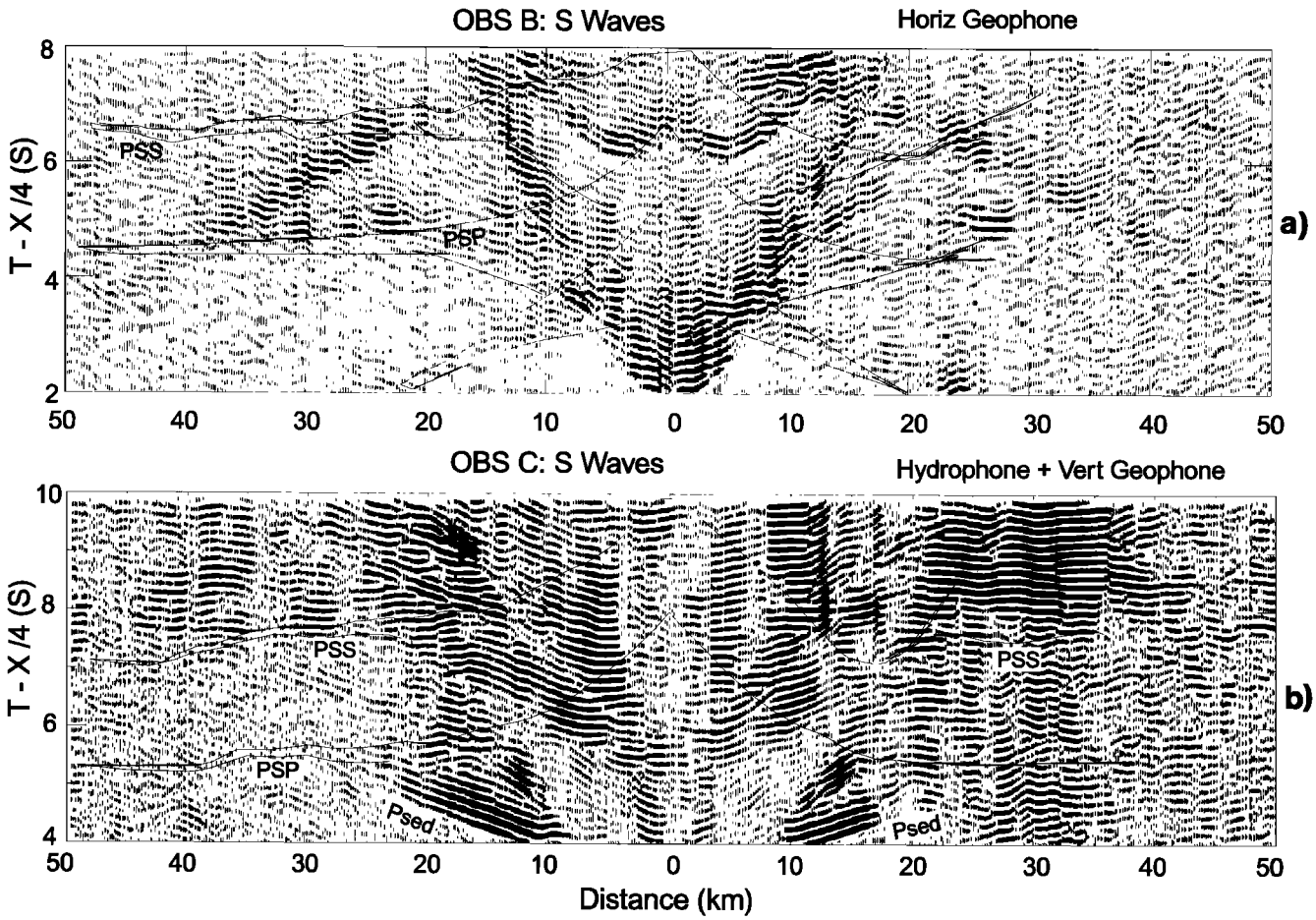

Figure 11. (a) Crustal *S* phases for the horizontal geophone channel of OBS B and (b) a combination of hydrophone and vertical geophone channels of OBS C. PSP is a crustal *S* refraction generated by double *P-S* conversion at the sediment/basement interface. PSS is converted only once at this interface.

For example, on the western margin of Iberia the lower crust near the proposed COB has anomalously high velocity (7.3-7.6 km/s) and a small thickness (2-3 km). This has been interpreted either as underplated melt [*Whitmarsh et al.*, 1990] or as serpentinite [*Boillot et al.*, 1992]. Farther south in the Tagus Abyssal Plain, even higher velocities (7.6-7.9 km/s) for the lower crust are interpreted as serpentinites [*Pinheiro et al.*, 1992]. On the conjugate margin off Newfoundland, refraction data on the southern Grand Banks show a thin, high-velocity (7.2-7.7 km/s), lower crust interpreted as serpentinite [*Reid*, 1994]. A similar high-velocity, lower crust is observed on the southern [*Todd and Reid*, 1989] and northern margins of Flemish Cap [*Reid and Keen*, 1990], but it is interpreted as underplated melt.

Among the two possible explanations for the origin of the high-velocity layer, the melt model is favored by the widely accepted existence of magmatic underplating immediately underneath the stretched lower continental crust of volcanic margins [*White and McKenzie*, 1989]. However, for a crystallized melt to have a velocity as high as 7.5 km/s, a high asthenospheric temperature is required, which for a stretching factor of >5 would have produced a minimum thickness of 20 km. Such a large thickness is not observed. A melt model also would require extrusive volcanics (e.g., seaward-dipping reflectors), a feature absent from reflection profiles across the margins of the Labrador Sea [*Balkwill*, 1987; *Keen et al.*, 1994]. In addition, a melt model cannot explain why our observed high-velocity layer is offset seaward by 80 km from the continental slope, where underplating is generally observed.

For the above reasons, we suggest that the observed high-velocity lower crust more likely represents a serpentinized mantle. The observed V_p - V_s for the lower crust of zone II (Figure 13) is consistent with the theoretical curve for ~15% serpentinization. Above the seismic Moho, the modified mantle has been "undercrusted" to form the high-velocity lower crust [*Boillot et al.*, 1989a,b]. A small amount of serpentinization also possibly exists within the upper mantle layer, increasing its vertical velocity gradient and producing a strong refracted arrival P_n (Figure 6). The basement high, bordering zones I and II, may represent a serpentinite diaper. It lies on top of the most highly serpentinized lower crustal layer where the velocity is lower than on either side (Figure 10a). Compared with the serpentinized ridge off Galicia margin [*Boillot et al.*, 1992], however, greater along-strike variations probably exist for the serpentinite diapir off SW Greenland, as evidenced by its reduced elevation on a nearby deep multichannel reflection profile (*Keen et al.*, 1994).

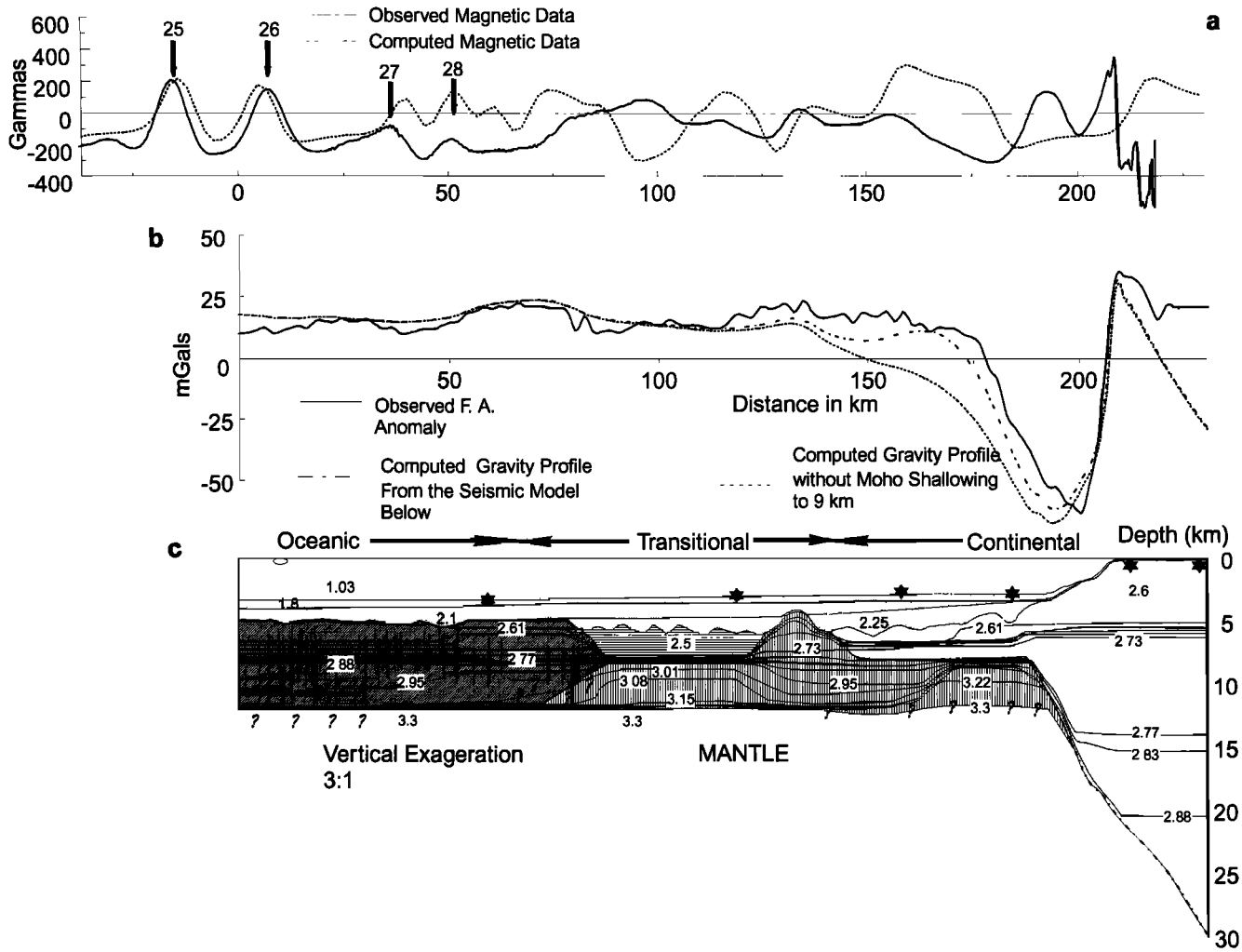

Figure 12. The modeling of magnetic and gravity data across the SW Greenland continent margin. (a) Observed magnetic data (solid line) along with computed curve (dotted line). The spreading rate and direction are from *Roest and Srivastava* [1989] using the time scale of *Kent and Gradstein* [1986]. (b) Observed free air anomaly (solid line) along with computed gravity profile (dashed line) calculated from the two-dimensional density model shown in (c). Dotted line is computed anomaly assuming a flat Moho at a depth of 11.8 km. (c) Two-dimensional density model. The density in the crust is calculated from the two-dimensional seismic model (Figure 10a) according to the relationship $\rho = -.6997 + 2.2302V - .598V^2 + .07036V^3 - .0028311V^4$ [*Ludwig et al.*, 1971]. Gravity contours follow velocity contours except for the leftmost 50 km.

Processes of Crustal Thinning

The major characteristics of the upper crust in zone II are its low velocity (4.0-5.0 km/s), its small thickness (~2.5 km), its blocky faulted pattern, and the irregular magnetic anomalies it generates (Figure 12). It cannot be oceanic crust (i.e., extruded mantle melt) if our interpretation of the underlying layer as serpentinized peridotite (as opposed to a plutonic intrusion) is correct. We suggest that the upper crust in zone II is composed of thinned and faulted upper continental crust. An approximate calculation of the stretching factor β based on the surface geometry of the tilted blocks suggests β=2-3 for this part of upper crust (Figure 2). From this value, the thickness of the preexisting continental crust is estimated to be 5-8 km. This is compatible with refraction data along the shelf of SW Greenland [*Chian and Louden*, 1992] and the depth of a reflector across the SW Greenland shelf in a nearby deep multichannel reflection profile (*Keen et al.*, 1994).

If the above interpretations are correct, the lower continental crust has been removed from this margin and must presently exist under the conjugate margin of Labrador. In the most basic form, this result suggests a simple shear model for the initial rifting [*Wernicke*, 1985; *Lister et al.*, 1986; *Wernicke and Tilke*, 1989], in which the SW Greenland margin acts as an upper plate and there is no associated magmatism. The very low angle normal fault that was responsible for the final breakup might have followed the present curvature of the Moho under the continental slope, turning almost horizontally at the base of the thinned continental crust for about 100 km (Figure 12). We do not know if the original lower continental crust beneath this fault was affected by syn-rift ductile creep, in addition to or instead of simple shear. To construct a complete rifting scenario, we require seismic data

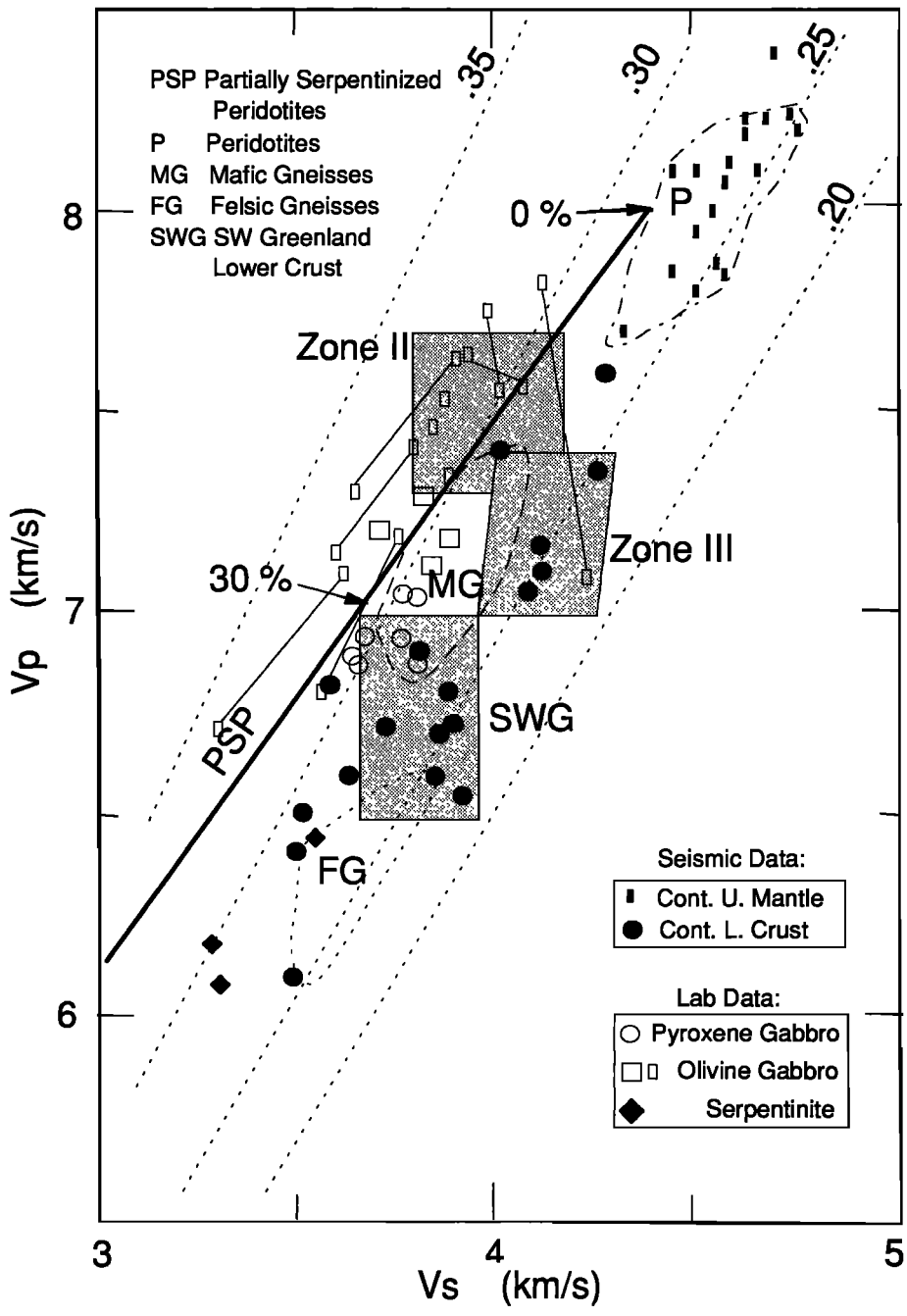

Figure 13. Compressional wave velocity versus shear wave velocity showing fields for peridotites (P); partially serpentinized peridotites (PSP) with 0 and 30 percent serpentine points marked; felsic gneisses (FG); mafic gneisses (MG); reported crustal seismic data for continental lower crust (solid circles) and upper mantle (vertical rectangles); and serpentinite data at 0.6 kbar from ophiolite samples (solid diamond) [*Fountain and Christensen*, 1989; *Christensen*, 1966, 1978, 1989]. Field for SWG represents the continental lower crust of the SW Greenland margin [*Chian and Louden*, 1992]. Also shown are laboratory data for pyroxene gabbro (open circles) and olivine gabbro (open rectangles) [*Spudich and Orcutt*, 1980a; *Christensen and Smewing*, 1981]. Fields for zones II and III are determined from the lower crustal seismic velocities and uncertainties (this paper).

on the conjugate Labrador margin. These data presently are being analyzed and will be presented in a subsequent paper.

Conclusions

Using wide-angle data and coincident normal-incidence seismic reflection data, we have obtained a detailed two-dimensional velocity model for the complete crustal transition of the sediment-starved, SW Greenland continental margin (Figure 10a). When converted to density values, this seismic model offers a reasonable fit to the gravity data (Figure 12). Interpretation of upper crustal structures is also compatible with the change in magnetic anomalies and character of basement structures.

The SW Greenland continental margin is characterized by three distinct zones:

1. In zone I, the 30-km preexisting continental crust is thinned abruptly to a thickness of ~3 km. This thinned crust is faulted and extends seaward to intersect a basement high, interpreted as an elevated serpentinized peridotite.
2. In the continent-ocean transition (zone II), the 4-5 km lower crust extends for 50-80 km and exhibits a bulk V_p of 7.5±0.1 km/s and V_s of 4.0±0.2 km/s. This is interpreted as undercrusted serpentinites. The faulted upper crust for this zone has a very low velocity of 4.0-5.0 km/s and possibly represents block-faulted upper continental crust.
3. The lower crust in zone III has V_p of ~7.2 km/s and V_s of ~4.1 km/s. Such velocities possibly extend seaward to the extinct ridge axis, and correspond to magnetic anomalies younger than chron 28. Seafloor spreading likely did not start until chron 28.
4. A simple shear model without magmatism is favored for the initial rifting of the Labrador Sea. The SW Greenland margin possibly acts as an upper plate margin, while the lower plate lies on the conjugate Labrador margin. Seismic data across the conjugate margin of Labrador are needed to further test the rifting model.

Appendix: Error Analysis of the Seismic Velocity Model

In this section we investigate the errors of velocity and depth obtained from the two-dimensional seismic modeling. We proceed by choosing a single layer, assuming that all the model parameters above this layer are accurate. We then perturb the depth and velocity for the top boundary of the layer by dZ_0 and dV_0 and perturb the depth and velocity gradient for the bottom boundary by dZ_1 and dg. It is clear that the

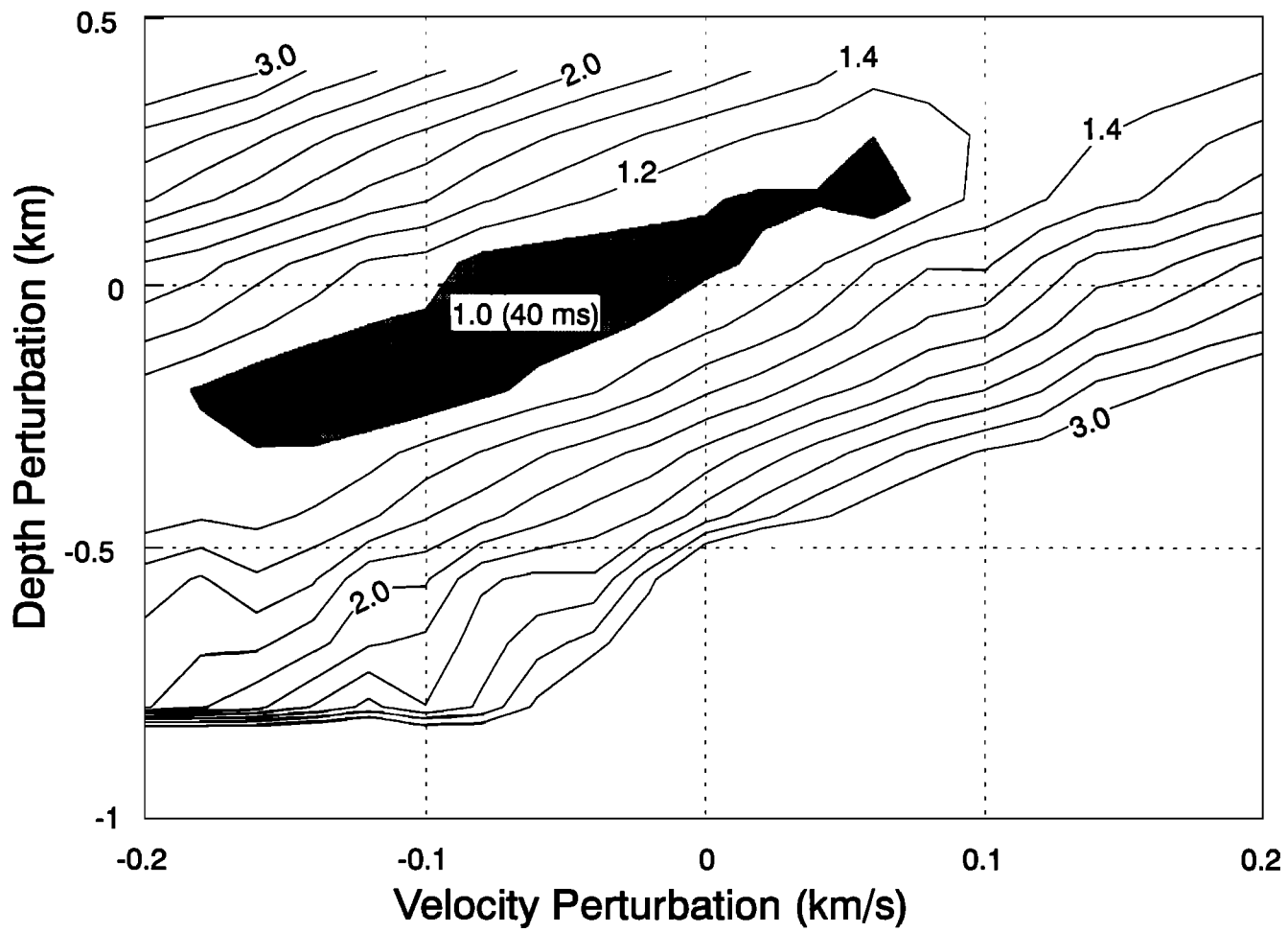

Figure A1 χ^2 contour plot for perturbations of velocity and depth for the seismic phase P_3 west of OBS C (Figure 6). The contours are normalized to the travel time endurance (maximum errors in observed travel time) of 40 ms. The area enclosed by χ^2=1 delimits error bounds for the velocity and depth for the lower crust.

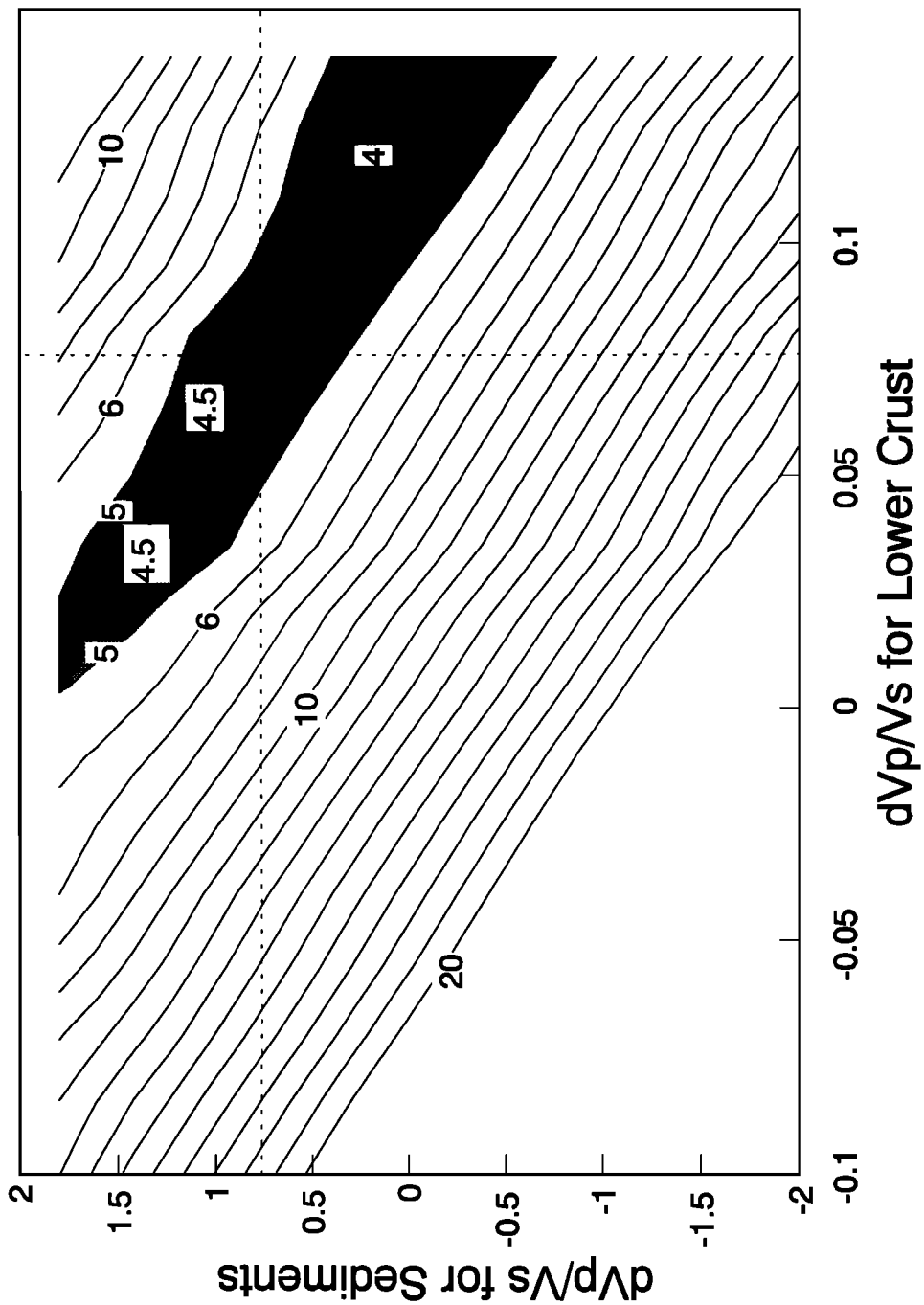

Figure A2. χ^2 contour plot for perturbations of V_p/V_s ratios in the lower crust and in the topmost sediment. The seismic phase for this error analysis is S_3 for the western ranges of OBS C (Figure 11b). The starting model has V_p/V_s ratios of 1.83 for the lower crust and 4.5 for the top sediment layer, respectively. No S waves can be generated for $d(V_p/V_s)>0.14$. The contours are normalized to 35 ms. This plot indicates that the preferred ratio for V_p/V_s is 1.91±0.10. The larger values of χ^2 suggest a further uncertainty due to limitations in the modeling procedure (see discussion in text).

refracted phase mainly controls dZ_0 and dV_0 and that the wide-angle reflection from the bottom boundary mainly controls dZ_1 and dg. Almost all the seismic travel time information about this layer is included in these two seismic phases. The exact travel time error analysis for the layer parameters is thus five dimensional (dZ_0, dZ_1, dV_0, dg, and the root-mean-square travel time misfit, T_{rms}). To simplify things, we performed the error analysis for one phase at a time, that is, a (dZ_0, dV_0 and T_{rms}) contour plot for the refracted (diving) phase within the layer (omitting the less sensitive parameter dg) and a (dZ_1, dg and T_{rms}) contour plot for wide-angle reflections from the bottom of the layer (assuming V_0 is accurate and therefore dV_0=0).

To quantify the error bounds of model parameters, a χ^2 misfit is used instead of T_{rms}, where

$$\chi^2 = \frac{T_{rms}}{U_0} = \frac{1}{U_0}\left(\frac{1}{n}\sum_{i=1}^{n}(To_i - Tc_i)^2\right)^{1/2}.$$

To_i and Tc_i are the observed and calculated travel times at selected points (i=1, 2, ... n) of a specific seismic phase whose travel time pick has an uncertainty of Uo (assumed to be constant for all i). For values of $\chi^2 \leq 1$, the computed and observed arrivals agree within the observed uncertainties of the travel times. This criteria may be used for defining error bounds of velocity, depth, and gradients. The bounds might be reduced further when consistent amplitude patterns are modeled in addition to travel times and where multiple raypaths from different receivers overlap.

In the implementation of the error analysis for the refracted phase, the perturbation of Z_0 is set to be uniform along the top boundary so that for all iterations the boundary relief is kept the same. The perturbation of V_0 is constant throughout the layer so that there is no gradient change during iterations. The errors of the gradient can be estimated by the second approach for wide-angle reflections in which g and Z_1 are varied. Figure A1 shows a χ^2 contour plot for the phase P_3 which is refracted from the high-velocity, lower crust for the final model in Figure 10a.

A similar approach can be used for the error analysis of S waves such as the PSP phase which is doubly converted at the sediment/basement interface. For PSS phases, with only a single P-S conversion, the method for error analysis is different because an extra unknown V_{sed}, the S velocity in the sediments, is introduced. In this instance, we replace the less sensitive variable, the depth perturbation dZ_0, with a perturbation of V_s in the sediment. Figure A2 shows a χ^2 contour plot of $d(V_p/V_s)$ for the lower crust and $d(V_p/V_s)$ for the topmost sediments. Here we use the ratio $d(V_p/V_s)$ instead of V_s alone for model iterations in order to retain the model variations obtained from the generally better resolved P waves. However, this method results in minimum χ^2 values of ~4, indicating that strict adherence to the P wave model and a uniform V_p/V_s ratio within each layer does not result in calculated S wave travel times that are able to fit the observations within their estimated uncertainties. This suggests either that our estimated uncertainties in the observed travel times are too low or that the V_p/V_s ratio varies within the layers, increasing the uncertainty in V_s.

Knowing the errors of V_p and V_s, the errors of Poisson's ratio $d\sigma$ can be estimated. Differentiating

$$\sigma = \frac{1}{2} - \frac{1}{2}\frac{V_s^2}{V_p^2 - V_s^2},$$

yields

$$|d\sigma| = \frac{\left|V_p V_s^2 dV_p - V_s V_p^2 dV_s\right|}{\left(V_p^2 - V_s^2\right)^2} \leq \frac{V_p V_s^2 |dV_p| + V_s V_p^2 |dV_s|}{\left(V_p^2 - V_s^2\right)^2}.$$

If V_p=7.5 km/s, $dV_p = \pm 0.1$ km/s, V_s=4.0 km/s, and $dV_s = \pm 0.2$ km/s, the above formula gives $\sigma = 0.30 \pm 0.03$.

Acknowledgments. This work was supported by grants from the National Science and Engineering Research Council and the Department of Energy, Mines, and Resources, Canada. D. Chian was partially supported by a Graduate Fellowship from Dalhousie University. We would like to thank the officers and crew of the C.S.S. Hudson and Borden Chapman, Guy Fehn, Martin Uyesugi, and Neil Hamilton for helping to collect the seismic data. Much of the instrumentation used at sea was on loan from the Atlantic Geoscience Centre, Bedford Institute of Oceanography. Data from the ocean bottom seismometers were digitized at the Bedford Institute of Oceanography with the help of Steve Perry. We thank S. Srivastava for supplying the sonobuoy F seismic data and C. Keen for early access to a deep multichannel reflection profile. Discussions with and comments on the manuscript from J. Osler, S. Srivastava, C. Keen, I. Reid, S. Holbrook, and an anonymous reviewer have been useful.

References

Balkwill, H.R., Labrador Margin: Structural style and evolution, *Mem. 12*, edited by C. Beaumont and A.J. Tankard, pp. 17-43, Can. Soc. of Petrol. Geol., Calgary, 1987.

Boillot, G., J. Girardeau, and J. Kornprobst, Rifting of the Galicia Margin: Crustal thinning and emplacement of mantle rocks on the seafloor, *Proc. Ocean Drill. Program Sci. Results, 103*, 741-756, 1988.

Boillot, G., J., G. Feraud, M. Recq, and J. Girardeau, "Undercrusting" by serpentinite beneath rifted margins: The examples of the west Galicia margin (Spain), *Nature, 341*, 523-525, 1989a.

Boillot, G., D. Mougenot, J. Girardeau, and E.L. Winterer, Rifting processes on the west Galicia margin, Spain, in Extensional Tectonics and Stratigraphy of the North Atlantic Margins, *Mem. 46*, edited by A.J. Tankard and H.R. Balkwill, pp. 363-377, Am. Assoc. Petrol. Geol., Tulsa, Okla., 1989b.

Boillot, G., J., M.O. Beslier, and M. Comas, Seismic image of undercrusted serpentinite beneath a rifted margin, *Terra Nova, 4*, 25-33, 1992.

Cerveny, V., I.A. Molotkov, and I. Psencik, *Ray Method in Seismology*, 214 pp., University of Karlova, Prague, 1977.

Chalmers, J.A., New evidence on the structure of the Labrador Sea/Greenland continental margin, *J. Geol. Soc., London, 148*, 899-908, 1991.

Chenet, P.-Y., L. Montadert, H. Gairaud, and D. Robert, Extension ratio measurements on the Galicia, Portugal and northern Biscay continental margins: Implications for evolutionary models of passive continental margins, in Studies in Continental Margin Geology, *Mem. 34*, edited by J.S. Watkins and C.L. Drake, pp. 703-715, Am. Assoc. Petrol. Geol., Tulsa, Okla., 1983.

Chian, D., and K.E. Louden, The structure of Archean/Ketilidian crust along the continental shelf of southwestern Greenland from a seismic refraction profile, *Can. J. Earth Sci., 29*, 301-313, 1992.

Christensen, N.I., Elasticity of ultramafic rocks, *J. Geophys. Res., 71*, 5921-5931, 1966.

Christensen, N.I., Ophiolites, seismic velocities and oceanic crustal structure, *Tectonophysics, 47*, 131-157, 1978.

Christensen, N.I., Seismic velocities, in Practical Handbook of Physical Properties of Rocks and Minerals, edited by R.S. Carmichael, pp. 429-546, CRC Press, Boca Raton, Fla., 1989.

Christensen, N.I., and J.D. Smewing, Geology and seismic structure of the northern section of the Oman Ophiolite, *J. Geophys. Res., 86*, 2545-2555, 1981.

Fountain, D.M., and N.I. Christensen, Composition of the continental crust and upper mantle: A review, in Geophysical Framework of the Continental United States Boulder, Colorado, Mem. 172, edited by L.C. Pakiser and W.D. Mooney, pp. 711-742, Geol. Soc. of Am., Boulder, Colo., 1989.

Ginzburg, A., R.B. Whitmarsh, D.G. Roberts, L. Montadert, A. Camus, and F. Avedik, The deep seismic structure of the northern continental margin of the Bay of Biscay, *Ann. Geophys., 3*, 499-510, 1985.

Gohl, K. and S.B. Smithson, Structure of Archean crust and passive margin of Southwest Greenland from seismic wide-angle data, *J. Geophys. Res., 98*, 6623-6638, 1993.

Holbrook, W.S., E.C. Reiter, G.M. Purdy, D. Sawyer, P.L. Stoffa, J.A. Austin Jr., J. Oh, and J. Makris, Deep structure of the U.S. Atlantic continental margin, offshore South Carolina, from coincident ocean-bottom and multichannel seismic data, *J. Geophys. Res.*, in press, 1994.

Horsefield, S.J., R.B. Whitmarsh, R.S. White, and J.-C. Sibuet, Crustal structure of the Goban Spur passive continental margin - Results of a detailed seismic refraction survey, *Geophys. J. Int.*, in press, 1994.

Jarrard, R.D., K.A. Dadey, and W.B. Busch, Velocity and density of sediments of Eirik Ridge, Labrador Sea: Control by porosity and mineralogy, *Proc. Ocean Drill. Program Sci. Results, 105*, 811-835, 1989.

Keen, C.E., and B. de Voogd, The continent-ocean boundary at the rifted margin off eastern Canada: New results from deep seismic reflection studies, *Tectonics, 7*, 107-124, 1988.

Keen, C.E., C. Peddy, B. de Voogd, and D. Matthews, Conjugate margins of Canada and Europe: Results from deep reflection profiling, *Geology, 17*, 173-176, 1989.

Keen, C.E., P. Potter, and S.P. Srivastava, Deep seismic reflection data across the conjugate margins of the Labrador Sea, *Can. J. Earth Sci.*, in press, 1994.

Kent, D.V., and Gradstein, F.M., A Jurassic to recent chronology, in *The Western North Atlantic Region, The Geol. of N. Am.*, vol. M, edited by P.R. Vogt and B.E. Tucholke, pp. 379-404, Geol. Soc. of Am., Boulder, Colo., 1986.

Le Pichon, X., and F. Barbier, Passive margin formation by low-angle faulting with the upper crust: The northern Bay of Biscay margin, *Tectonics, 6*, 133-150, 1987.

Lister, G.S., M.A. Ethridge, and P.A. Symonds, Detachment faulting and the evolution of passive continental margins, *Geology, 14*, 246-250, 1986.

Ludwig, W.J., J.E. Nafe, and C.L. Drake, Seismic refraction, in *The Sea*, vol. 4, edited by A.E. Maxwell, pp. 53-84, Wiley-Interscience, New York, 1971.

McKenzie, D.P., Some remarks on the development of sedimentary basins, *Earth Planet. Sci. Lett., 40*, 25-32, 1978.

Mutter, J.C., M. Talwani, and P.L. Stoffa, Evidence for a thick oceanic crust adjacent to the Norwegian margin, *J. Geophys. Res., 89*, 483-502, 1984.

Osler, J., Crustal structure of the extinct spreading centre in the Labrador Sea: Implications for dynamic models of Flow beneath Mid-Ocean Ridges, Ph.D. Thesis, 200 pp., Dalhousie Univ., Halifax, Nova Scotia, 1993.

Osler, J., and K.E. Louden, Crustal structure of an extinct rift axis in the Labrador Sea: Preliminary results from a seismic refraction survey, *Earth Planet. Sci. Lett., 108*, 243-258, 1992.

Peddy, C., B. Pinet, D. Masson, R. Scrutton, J.-C. Sibuet, M.R. Warner, J.-P. Lefort, and I.J. Shroeder, Crustal structure of the Goban Spur continental margin, Northeast Atlantic, from deep seismic reflection profiling, *J. Geol. Soc. London, 146*, 427-437, 1989.

Pinheiro, L.M., R.B. Whitmarsh, and P.R. Miles, The ocean-continent boundary off the western continental margin of Iberia, II, Crustal structure in the Tagus Abyssal Plain, *Geophys. J. Int., 109*, 106-124, 1992.

Reid, I.D., Crustal structure of a nonvolcanic rifted margin east of Newfoundland, submitted to *J. Geophys. Res.*, 1994.

Reid, I.D., and C.E. Keen, High seismic velocities associated with reflections from within the lower oceanic crust near the continental margins of eastern Canada, *Earth Planet. Sci. Lett., 99*, 118-126, 1990.

Roest, W.R., and S. P. Srivastava, Sea-floor spreading in the Labrador Sea: A new reconstruction, *Geology, 17*, 1000-1003, 1989.

Rolle, F., Late Cretaceous-Tertiary sediments offshore central West Greenland: Lithostratigraphy, sedimentary evolution and petroleum potential, *Can. J. Earth Sci., 22*, 1001-1019, 1985.

Sibuet, J.-C., Formation of nonvolcanic passive margins: A composite model applied to the conjugate Galicia and southeastern Flemish Cap margins, *Geophys. Res. Lett., 19*, 769-772, 1992.

Spudich, P., and J. Orcutt, A new look at the seismic velocity structure of the oceanic crust, *Rev. Geophys. Space Phys., 18*, 627-645, 1980a.

Spudich, P., and J. Orcutt, Petrology and porosity of an oceanic crustal site: Results from wave form modeling of seismic refraction data, *J. Geophys. Res., 85*, 1409-1433, 1980b.

Srivastava, S.P., Evolution of the Labrador Sea and its bearing on the early evolution of the North Atlantic, *Geophys. J. R. Astron. Soc., 52*, 313-357, 1978.

Srivastava, S.P., K. E. Louden, S. Chough, D. Mosher, B. D. Loncarevic, P. Mudie, A. de Vernal, and B. Maclean, Results of detailed geological and geophysical measurements at ODP sites 645 in Baffin Bay and 646 and 647 in the Labrador Sea, *Proc. Ocean Drill. Program Sci. Results, 105*, 891-922, 1989.

Stergiopolous, A.B., *Geophysical Crustal Studies off the Southwest Greenland Margin*, M.Sc. thesis, 250 pp., Dalhousie Univ., Halifax, Nova Scotia, 1984.

Todd, B.J., and I. Reid, The continent-ocean boundary south of Flemish Cap: Constraints from seismic refraction and gravity, *Can. J. Earth Sci., 26*, 1392-1407, 1989.

Tucholke, B., Sediment distribution, in *Geophysical Atlas of the North Atlantic between 50° to 72° N and 0° to 65° W*, edited by S.P. Srivastava, D. Voppel, and B. Tucholke, pp. 9-12, Dsch. Hydrog. Inst., Hamburg, 1988.

Van der Linden, W.J.M., Crustal attenuation and sea-floor spreading in the Labrador Sea, *Earth Planet. Sci. Lett., 27*, 409-423, 1975.

Voppel, D., R. Rudloff, J. Schulz-Ohlberg, S.P. Srivastava, K.G. Shih, P.D. Rabinowitz, and W. Jung, Free air gravity anomalies, in *Geophysical Atlas of the North Atlantic between 50° to 72° N and 0° to 65° W*, edited by S.P. Srivastava, D. Voppel, and B. Tucholke, pp. 5-8, Dsch. Hydrog. Inst., Hamburg, 1988.

Watt, W.S., The coast-parallel dike swarm of southwest Greenland in relation to the opening of the Labrador Sea, *Can. J. Earth Sci., 6*, 1320-1321, 1969.

Wernicke, B., Uniform-sense normal simple shear of the continental lithosphere, *Can. J. Earth Sci., 22*, 108-125, 1985.

Wernicke, B., and P. G. Tilke, Extensional tectonic framework of the U.S. Central Atlantic passive margin, in Extensional Tectonics and Stratigraphy of the North Atlantic Margins, Mem. 46, edited by A.J. Tankard and H.R. Balkwill, pp. 7-21, Am. Assoc. of Petrol. Geol., Tulsa, Okla., 1989.

White, R., and D. McKenzie, Magmatism at rift zones: The generation of volcanic continental margins and flood basalts, *J. Geophys. Res., 94*, 7685-7729, 1989.

Whitmarsh, R. B., F. Avedik, and M.R. Saunders, The seismic structure of thinned continental crust in the northern Bay of Biscay, *Geophys. J. R. Astron. Soc., 86*, 589-602, 1986.

Whitmarsh, R.B., P.R. Miles, and A. Mauffret, The ocean-continent boundary off the western continental margin of Iberia, I, Crustal structure at 40°30'N, *Geophys. J. Int., 103*, 509-531, 1990.

Woodside, J., Gravity anomaly in Labrador Sea, in *Labrador Sea Atlas, East Coast Basin Atlas Ser.*, edited by J. S. Bell, pp. 94-95, Geol. Surv. of Can., Dartmouth, Nova Scotia, 1989.

D. Chian and K. E. Louden, Dalhousie University, Department of Oceanography, Halifax, Nova Scotia, Canada B3H 4J1. (e-mail: qian1@ac.dal.ca, Deping Chian)

(Received February 3, 1993; revised September 22, 1993; accepted November 30, 1993.)